ANALYTICAL AND NUMERICAL MODELING OF EXTERNALLY HEATED GEOTHERMAL BRIDGE DECK

by

MANDAKINI CHOWDHURY

Presented to the Faculty of the Graduate School of

The University of Texas at Arlington in Partial Fulfillment

of the Requirements

for the Degree of

MASTER OF SCIENCE IN CIVIL ENGINEERING

THE UNIVERSITY OF TEXAS AT ARLINGTON

August 2019

Acknowledgments

First and foremost, I would like to extend my gratitude to my academic advisor and thesis supervisor, Dr. Xinbao Yu, for his inspiration, assistance and vital inputs during my graduate career. This thesis would be incomplete without his constant guidance, critical inputs and patient support.

I would also like to thank Dr. Sahadat Hossain and Dr. Nilo Tsung for their consent to serve in my committee and offer their time and precious suggestions. I sincerely acknowledge the team members in my research group their co-operation during the entire graduate studies.

I am indebted to Mark Hurley, Omid Habibzadeh Bigdarvish, Gang Lei, Teng Li, Rakib Hasan, Dr. Jobair Bin Alam, Dr. Naima Rahman, Ashrafuzzaman Khan, Umme Zakira and Fatema Ruma for their invaluable support during my graduate studies.

Last but by no means the least, I sincerely convey my deepest gratitude to my parents, Ranjit Kumar Chowdhury and Monjusree Chowdhury, my siblings, my parents in-law, and specially my beloved husband, Arindam Dhar, for their motivation and for being an inspiration to all my success.

July 22, 2019

Abstract

ANALYTICAL AND NUMERICAL MODELING OF EXTERNALLY HEATED GEOTHERMAL BRIDGE DECK

Mandakini Chowdhury

The University of Texas at Arlington, 2019

Supervising Professor: Dr. Xinbao Yu

Bridge icing is a severe safety concern for travel during winter months in the United States. Ice on bridges form quicker than roads, as the bridge is exposed to wind on all its surfaces. The underlying problem of bridge icing is loss of friction between the vehicle wheel and the pavement surface due to slippery nature of ice. Hence, the solution is to increase the friction between the above-mentioned surfaces. The most commonly adopted solution is application of sand, salt or other granular materials on the roadway. However, due to corrosive nature of the salts, the durability of the infrastructure is affected. Hence, alternative pavement de-icing technologies are becoming popular, playing an important role in transportation safety and environmental protection. One of the sustainable bridge de-icing options is a ground source heat pump (Zhang, Yu, & Li, 2017; Li, Lei, Zhang, & Puppala, 2018). The theoretical principle of this technique is exploitation of relative constant temperature and heat storage capacity at around 10-30 feet underground and use of this heat storage capacity as a heat source for slab de-icing in winter (Bowers and Olgun, 2014; Li, et al., 2018). This heat source, coupled with hydronic loops embedded inside the bridge deck, acts as a de-icing system for the bridge decks. TxDOT is currently investigating the potential of using hydronic system in the highway bridge decks to counter the bridge icing problem in Dallas-Fort Worth (DFW) Area. Therefore, a numerical model needs to be developed and the local weather variables need to be simulated to evaluate the de-icing efficiency of the proposed hydronic

system in Dallas-Fort Worth (DFW) Area.

In the current study, an experimental bridge deck, along with the hydronic system attached to the bottom of the deck slab, was set up by the geothermal research group under the supervision of Dr. Xinbao Yu. The performance of the system was evaluated in actual weather conditions by monitoring the temperature of the installed thermocouples at different locations within the slab with respect to ambient temperature and wind speed. Based on the experimental design, a numerical model was developed in COMSOL and the model was validated by thermocouple data obtained from the experimental deck slab. With the validated numerical model, performance of the proposed system was evaluated by simulating the coldest days of last five years (2014-2018) and monitoring the slab temperature on the model. The effect of using insulated foam at the bottom of the bridge deck was also investigated. An analytical thermal resistance model was also developed to determine the consistency between the experimental, numerical and theoretical results obtained during the study. Based on the results obtained during the study, it can be concluded that the proposed hydronic system is adequate to prevent ice formation on bridge decks in DFW area.

TABLE OF CONTENTS

List of Figures

List of Tables

Chapter 1.
INTRODUCTION

1.1 Background

Bridge icing is a severe safety concern for travel during winter months in the United States. Ice on bridges form quicker than roads, as the bridge is exposed to wind on all its surfaces. In contrast, roadway is only exposed to wind on its top surface, reducing icing potential. The most dangerous aspect of icing on bridge is that it is virtually undetectable and very similar in appearance to a wet road. Lack of visual warning leads to drivers approaching ice at full speed and eventual loss of control of vehicle, which is catastrophic. The risk of accident is compounded due to low visibility during a freezing rain event, which leads to a chain of accidents, traffic disruptions and even loss of lives.

The underlying problem of bridge icing is loss of friction between the vehicle wheel and the pavement surface due to slippery nature of ice. Hence, the solution is to increase the friction between the above-mentioned surfaces. The most commonly adopted solution is application of sand, salt or other granular materials on the roadway. However, timing of sand or salt application is complex. Moreover, the corrosive nature of salt is detrimental to reinforcing steel and service life of bridge decks. Alternative non-corrosive materials add significant cost to the maintenance operations (Spitler & Ramamoorthy, 2000).

An alternative, sustainable solution to the bridge icing problem is use of hydronic heating system, involving a ground source heat pump and polyethylene pipe (PEX) arranged in a meandering configuration embedded in the deck slab. The underlying principle of this method is heat transfer from the heated water to the pipe and from pipe to the deck slab by convection and conduction respectively. Hydronic heating is the preferred method between other comparable alternatives (heat pipe system, electric heating etc.) due to flexibility of heat source selection, higher energy efficiency, ease of construction and economic viability (Liu, 2005; Habibzadeh-Bigdarvish, Yu, Lei, Li, & Puppala, 2019).

1.2 Problem Statement

Hydronic heating is a preferred method of de-icing bridges among many alternatives. However, embedment of pipe in the deck slab makes construction more challenging and expensive.

TxDOT is currently investigating the potential of using hydronic system in the highway bridge decks to counter the bridge icing problem in Dallas-Fort Worth (DFW) Area. A unique approach is proposed for installing the hydronic system, where the pipes will be attached to the bottom of the deck slab instead of being embedded into the slab. This would dramatically reduce construction challenges, and cost of installation and maintenance of the system will also be reduced due to easy access to the system at the bottom of the slab. However, the efficiency of the system will be reduced as they will be susceptible to heat loss at the bottom. Hence, a layer of insulating foam encapsulation is proposed to minimize heat loss of the system to surroundings. Since the efficiency of the system is highly dependent on many interacting factors like heating capacity, local weather variation and extremities, large scale implementation of the system can only be justified if the efficiency of proposed external system in de-icing due to local weather conditions is reliably demonstrated. This objective can be satisfied by simulating the proposed hydronic system setup and local weather conditions of DFW area in a numerical model.

1.3 Research Objectives

The main objective of this study is to investigate the efficiency and adequacy of proposed hydronic system to achieve successful de-icing of the bridge. Since weather in ever changing, only one year's weather data is deemed inadequate to justify the efficiency of the bridge. Hence, the extreme weather events of five consecutive years (2014 – 2018) will be considered in this study for simulation purposes. The following tasks will be undertaken in this study to achieve the above-mentioned objectives:

I. Development of a numerical 3D COMSOL model that mimics an experimental bridge deck
II. Validation of numerical 3D COMSOL model by comparing numerical model outputs to experimental data for actual weather events
III. Prediction of de-icing efficiency of the proposed system in the extreme weather events of last 5 years in DFW area
IV. Compare the surface temperature calculated from a theoretical thermal resistance model to experimental thermocouple temperatures obtained during the study

1.4 Thesis Organization

This thesis consists of six chapters: Introduction (Chapter 1), Literature Review (Chapter 2), Experimental Program (Chapter 3), Numerical Modeling in COMSOL (Chapter 4), Results & Discussion (Chapter 5), and Conclusions & Recommendation for future work (Chapter 6).

The first chapter introduces general information of the study, problem statement, research objectives and a brief outline of the thesis organization.

The second chapter highlights the literatures on heat transfer mechanisms, previous research on hydronic heating system models, historical bridge heating system models and their characteristics and limitations.

The third chapter discusses the experimental setup of the hydronic heating system installation and the design of the experiments based on the weather events. It also discusses the layout of the thermocouple arrangement inside the test slab, data collection methods and circulation system details adopted during the study. It elaborates on some of the experimental results obtained from the experimental setup.

The fourth chapter illustrates the conceptual design, the assigned material properties, the physics assigned to the model, along with the meshing details of the numerical model in COMSOL. The chapter also presents details to justify the physical model inputs to mimic the experimental setup.

The fifth chapter presents the test results obtained from the experimental setup in response to the weather events, the corresponding numerical model results and comparison between them. This chapter discusses the response of the numerical model to the historical weather data inputs and comparison between experimental data, numerical model outputs and analytical heat resistance model outputs developed during the study. The chapter also includes some prediction of the system performance based on historical weather data inputs in the verified COMSOL model.

The sixth chapter summarizes the conclusions of the entire study and presents some recommendations for subsequent research work.

Chapter 2.
LITERATURE REVIEW

2.1 Introduction

De-icing bridge decks and pavement slabs is the foremost priority to maintain uninterrupted traffic flow during winter season. Some common methods used to counter icing problem are de-icers like Sodium Chloride, Calcium Chloride and Magnesium Chloride, applied directly to the pavement surface. However, chloride ions have corrosive effects, having potentially harmful effects on durability of the structure, soil properties and underground water resources (Li, et al., 2018). Hence, alternative pavement de-icing technologies are becoming popular, playing an important role in transportation safety and environmental protection. One of the sustainable bridge de-icing options is a ground source heat pump (Zhang, Yu, & Li, 2017; Li, Lei, Zhang, & Puppala, 2018). The theoretical principle of this technique is exploitation of relative constant temperature and heat storage capacity at around 10-30 feet underground and use of this heat storage capacity as a heat source for slab de-icing in winter (Bowers & Olgun, 2014; Li, Lei, Zhang, & Puppala, 2018). Geothermal energy exploitation plays a crucial role in ground source heat pump system performance, which is affected by different factors such as coupled thermo-hydro processes in soil (Lei, Kaneza, Yu, Li, & Habibzadeh-Bigdarvish, 2019). However, this heat source, coupled with hydronic loops embedded inside the bridge deck, acts as a de-icing system for the bridge decks.

Hydronic heating is a preferred method of de-icing bridges among many alternatives. The basic working principle of hydronic heating is heat transfer from the heated fluid circulating in the embedded pipe to the slab surface to melt snow. This principle works in two stages: heat diffusion inside the slab due to heated fluid in embedded pipe and heat transfer at the interface between the slab surface and the external environment.

To understand the mechanism of hydronic heating system, a basic understanding of the heat transfer mechanism is necessary. Hence, this chapter is divided into two parts: a discussion

on the basic mechanism of heat transfer, followed by a study on the previously developed numerical models for heat transfer mechanism of bridge heat transfer mechanism. The following section (section 2.2) is based on the review of the corresponding topics from Bergman, Incropera, Lavine, & Dewitt (2011).

2.2 Heat transfer Mechanism

Heat Transfer is a discipline of thermal energy that is defined as the transfer of thermal energy between physical system due to temperature difference. Heat transfer is categorized into three basic mechanisms:

i) Heat conduction

ii) Heat convection and

iii) Heat radiation

Though these mechanisms have different properties, they often take place in the same system simultaneously.

Heat Conduction

Heat conduction is also denoted as diffusion that concerns the transfer of energy from the more energetic to the less energetic molecules through the boundary between two systems. When an object is at a different temperature from another object or its surrounding, heat transfer happens in such a way that both objects reach the thermal equilibrium. According to the second law of thermodynamics, energy transfer by conduction must occurs from a high temperature to lower temperature due to the temperature gradient.

For heat conduction, heat transfer rate equation is recognized as Fourier's law. For steady state conduction heat transfer through a plane wall (Figure 1) the conduction heat transfer rate is

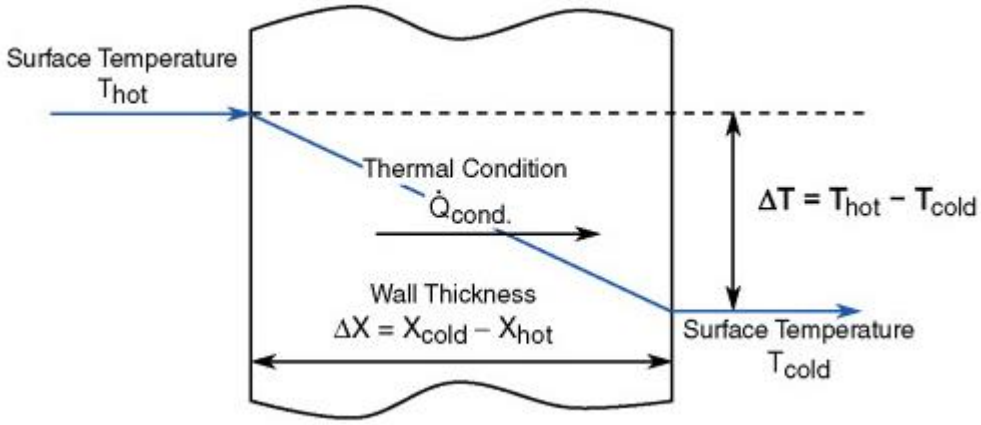

Figure 2.1 Thermal conduction through a wall (Kosky, Balmer, Keat, & Wise, 2015)

$$\dot{Q} = -KA\, dT/dx \qquad \text{(Equation 1)}$$

Where, $\dot{Q}$= conduction heat transfer rate and it is proportional to the temperature gradient dT/dx

K = Thermal conductivity of the material

A = Cross sectional area of the wall perpendicular to the heat transfer direction

The minus sign indicates transferring heat in the decreasing temperature direction.

Heat Convection

Convection heat transfer sometimes advection is defined as superposition of heat transfer due to the bulk motion of the molecules, also called diffusion and by bulk or microscopic movements within fluid such as gases, liquids. Convection heat transfer is a very complex part in heat transfer mechanism since here involves relative motion of the fluid and heat conduction.

As we described earlier, convection heat transfer occurs when fluid in motion and boundary surface are at different temperatures. Assuming fluid flow over the heated surface of figure (2 & 3). At the fluid-surface boundary interface where the fluid velocity varies from zero to a

finite value U∞ associated with the flow is known as the hydrodynamic, or velocity boundary layer. In this region random molecular motion (diffusion) governs near the surface where the velocity is nearly negligible. Moreover, there is another region called Thermal Boundary layer where temperature varies from Ts at y= 0 to T∞ between surface and flow temperature. In this region heat is transferred by bulk fluid motion as the boundary layer grows with the flow progress in the X direction. In any case, if Ts > T∞, convection heat transfer will take place.

For heat convection, heat transfer rate equation is known as Newton's law of cooling which is expressed as

$$q'' = h\,(T_s - T_\infty) \qquad \text{(Equation 2)}$$

Where, q''=Convective Heat Flux ($\frac{W}{m^2}$)

T_S=Surface temperature

T_∞=Fluid Temperature

"h" =Convective Heat Transfer Coefficient, which depends on boundary layer, nature of the fluid movements and fluid properties.

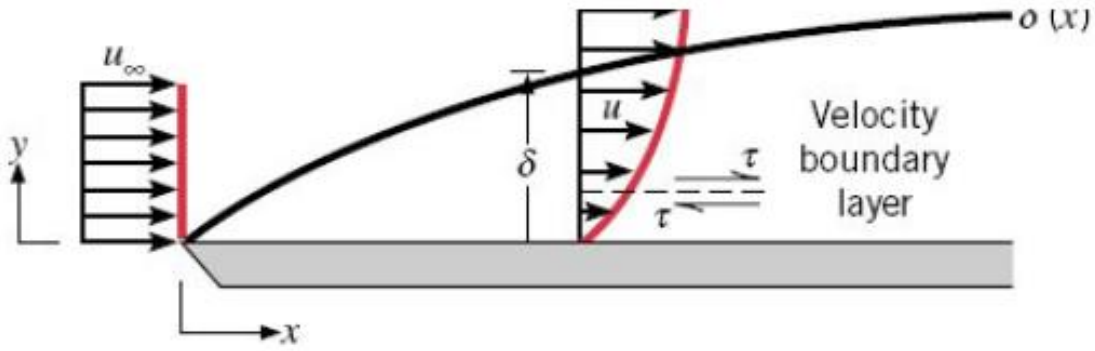

Figure 2.2 Velocity Boundary Layer Development on a flat plate (Bergman, Incropera, Lavine, &

Dewitt, 2011)

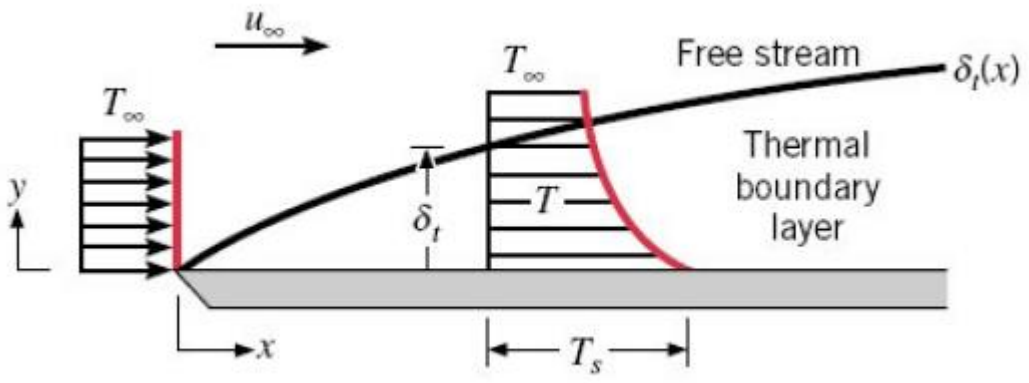

Figure 2.3 Thermal Boundary Layer development on an isothermal plate
(Bergman, Incropera, Lavine, & Dewitt, 2011)

Convection Mechanism

In heat transfer mechanism, convection transfer in fluid flows can be categorized into two types: free convection and forced convection.

In free convection, convection happens within the fluid irrespective of fluid velocity. In this mechanism, temperature gradient is created due to buoyancy force within the fluid. Buoyancy occurs due to the simultaneous presence of a fluid density gradient and a body force, which is proportional to the fluid density. In free convection, the heat transfer coefficient can be calculated from the Grashof Number.

In forced convection, the movement between the fluid and surface can be controlled by external means such as fan or pump but not by buoyancy force. The forced convection is a very complex part in thermodynamics. The mechanism of forced convection is categorized into two distinct categories, external flow and internal flow.

In external forced convection, an external means (pump, fan etc.) is responsible for fluid

flow over a surface or in a tube. However, in internal forced convection, fluid flow is forced in an enclosed pipe or tube.

Range of h value

A range of convective heat transfer coefficients (h) under different modes of convection are provided below (Bergman, Incropera, Lavine, & Dewitt, 2011)

Table 2.1 Range of convection values for different modes of convection
(Bergman, Incropera, Lavine, & Dewitt, 2011)

Type of Convection	**Convective heat ($W/m^2.k$)**
Free Convection of Gases	2 - 25
Free Convection of Liquids	10 - 1000
Forced convection of gases	25 - 250
Forced convection of liquids	50 - 20,000
Boiling and Condensation	2500 - 100,000

Heat Radiation

Thermal radiation is defined as emission of energy by matter that is at a finite temperature. Emission may also occur in liquid and gases. Exchange of energy in the radiation field is transported by electromagnetic waves. While radiation transfer occurs in a vacuum most effectively, heat transfer be conduction or convection requires a material medium. Additionally, the radiation or electromagnetic form where any substance at non-zero temperature releases energy and absorbs energy from surroundings following the same mechanism called irradiation.

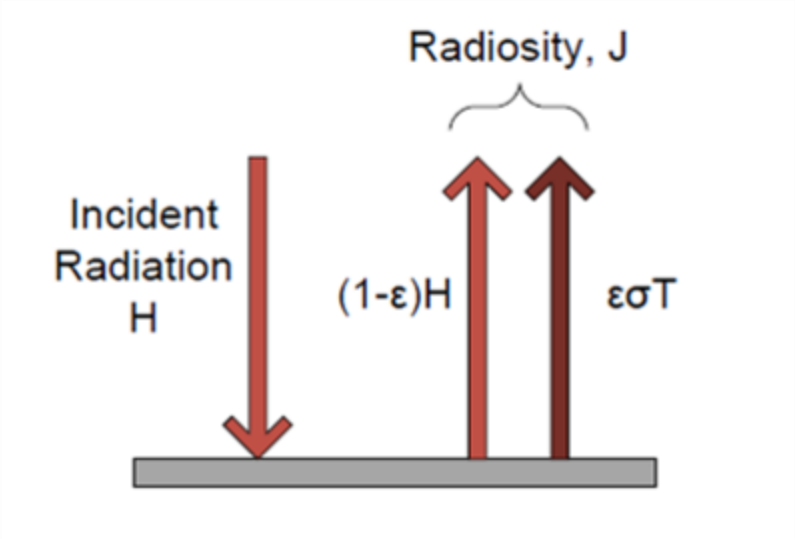

Figure 2.4 Incident Radiation and Radiosity (Wikipedia contributors, 2019, May 18)

Let us consider radiation transfer process for the surface. Radiation emitted by the surface comes from the thermal energy of matter surrounded by the surface and the rate at which energy is produced per unit area (W/m^2) is termed as the surface emissive power E. The emissive power is described by Stefan-Boltzmann Law (Equation 3).

$$E_b = \sigma T_s^4 \qquad \text{(Equation 3)}$$

Where, E_b =Surface Emissive Power

σ =Stefan Boltzmann Constant=5.67 $X10^{-8}$ $W/m^2. K^4$

Moreover, if the surface is supposed to be one for which $\alpha = \varepsilon$, radiation exchange between surfaces is expressed as

$$q = \in \alpha A_s (T_s^4 - T_{surr}^4) \qquad \text{(Equation 4)}$$

$$= h_{rad} (T_s^4 - T_{surr}^4)$$

The Conservation of Energy Requirement**:**

According to the first law of thermodynamics, it is stated that the amount of thermal and mechanical energy that enters a control volume plus the amount of thermal energy that is generated within the control volume, minus the amount of thermal and mechanical energy that leaves the control volume must equal the increase in the amount of energy stored in the control volume over the time interval (Equation 5)

$$E_{In} - E_{out} + E_{generated} = E_{stored} \qquad \text{(Equation 5)}$$

Heat diffusion equation

According to the principal of conservation of energy, let us consider a differential element in Cartesian coordinates, as shown in Figure 2.5.

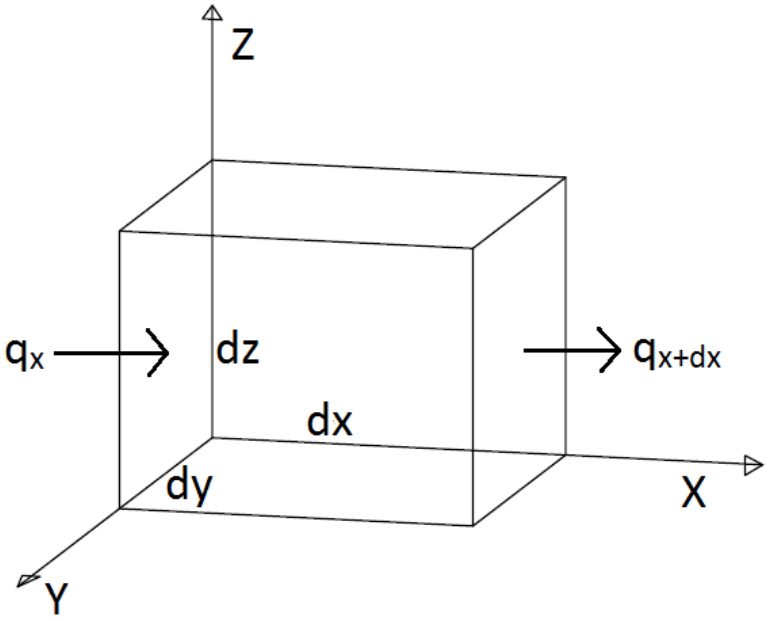

Figure 2.5 Representation of Heat Diffusion Equation (Lucid Learning, 2017, Jan 24)

The energy balance for the differential element can be described as

(Rate of heat conduction at X,Y,Z) - (Rate of heat conduction at x+dx, y+dy, z+dz)

+ (Rate of heat generation inside the element) = (Rate of change of energy content of the element)

After simplification, the general heat conduction equation in Cartesian Coordinates is expressed as

$$\frac{\partial}{\partial x}\left(k\frac{\partial T}{\partial x}\right)+\frac{\partial}{\partial y}\left(k\frac{\partial T}{\partial y}\right)+\frac{\partial}{\partial z}\left(k\frac{\partial T}{\partial z}\right)+q^{\cdot}=\rho c_p\frac{\partial T}{\partial t} \qquad \text{(Equation 6)}$$

Where, k = thermal conductivity of the material

ρ = Density

c_p= Specific heat

If conductivity K is constant, the equation will be

$$K\left(\frac{\partial^2 T}{\partial x^2}+\frac{\partial^2 T}{\partial y^2}+\frac{\partial^2 T}{\partial z^2}\right)+q^{\cdot}=\rho c_p\frac{\partial T}{\partial t} \qquad \text{(Equation 7)}$$

$$\text{Or, } \left(\frac{\partial^2 T}{\partial x^2}+\frac{\partial^2 T}{\partial y^2}+\frac{\partial^2 T}{\partial z^2}\right)+\frac{q^{\cdot}}{k}=\frac{\rho c_p}{k}\frac{\partial T}{\partial t}=\frac{1}{\alpha}\frac{\partial T}{\partial t} \qquad \text{(Equation 8)}$$

Where, α = Thermal Diffusivity

For steady state,

$$\left(\frac{\partial^2 T}{\partial x^2}+\frac{\partial^2 T}{\partial y^2}+\frac{\partial^2 T}{\partial z^2}\right)+\frac{q^{\cdot}}{k}=0 \qquad \text{(Equation 9)}$$

In case of no heat generation,

$$\left(\frac{\partial^2 T}{\partial x^2}+\frac{\partial^2 T}{\partial y^2}+\frac{\partial^2 T}{\partial z^2}\right)=0 \qquad \text{(Equation 10)}$$

And, for one dimensional analysis,

$$\frac{\partial^2 T}{\partial x^2} = 0 \text{ or may be } \frac{\partial}{\partial x}\left(k\frac{\partial T}{\partial x}\right)=0 \qquad \text{(Equation 11)}$$

Similarly, for cylindrical and spherical coordinates, the equation is expressed as

$$\frac{1}{r}\frac{\partial}{\partial r}\left(kr\frac{\partial T}{\partial r}\right)=0 \qquad \text{(Equation 12)}$$

$$\frac{1}{r^2}\frac{\partial}{\partial r}\left(kr^2\frac{\partial T}{\partial r}\right)=0 \qquad \text{(Equation 13)}$$

Thermal resistance in Cartesian coordinate system:

Thermal resistance is a very essential concept in thermodynamics. There exists a partial similarity between heat diffusion and electrical charge. Using electrical analogy in the heat transfer mechanism,

Current (I) → Heat Flow

Voltage (ΔV) → Temperature difference (ΔT)

Resistance (R) → Thermal Resistance (R_{th})

According to ohm's law,

$$\Delta V = IR \qquad \text{(Equation 14)}$$

Similarly,

According to Fourier law,

$$\Delta T = q\, R_{th} \qquad \text{(Equation 15)}$$

$$R_{th} = \frac{\Delta T}{q} \qquad \text{(Equation 16)}$$

The unit of thermal resistance = K/Watt.

Comparison of conduction $\boldsymbol{R_{th}}$ and electrical R:

Electrical Resistance

$$R \alpha \frac{1}{A}$$

Conduction Resistance

$$R \alpha \frac{1}{A}, L$$

$$R_{th} = \frac{L}{KA} \qquad \text{(Equation 17)}$$

Convection Resistance

$$R_{th} = \frac{1}{hA} \qquad \text{(Equation 18)}$$

Radiation Resistance

$$R_{th,r} = \frac{1}{h_r A} \qquad \text{(Equation 19)}$$

Thermal resistance for composite wall**:**

Similar thermal circuits may also be used for composite wall. These types of wall consist of series and parallel thermal resistance due to variation in wall materials. Consider 1D heat transfer rate for the wall (Figure 6). The 1D heat transfer rate for this system may be described as

-

$$q = \frac{T_{\infty,1} - T_{\infty,2}}{R_{total}} \qquad \text{(Equation 20)}$$

Where, $T_{\infty,1} - T_{\infty,2}$ = the overall temperature difference

R_{total} = total thermal resistance

$$q = \frac{T_{\infty,1} - T_{\infty,2}}{\frac{1}{h_1 A} + \frac{L}{KA} + \frac{1}{h_2 A}} \qquad \text{(Equation 21)}$$

$$q = \frac{T_{\infty,1} - T_{s,1}}{\frac{1}{h_1 A}} = \frac{T_{s,1} - T_{s,2}}{\frac{L}{KA}} = \frac{T_{s,2} - T_{\infty,2}}{\frac{1}{h_2 A}} \qquad \text{(Equation 22)}$$

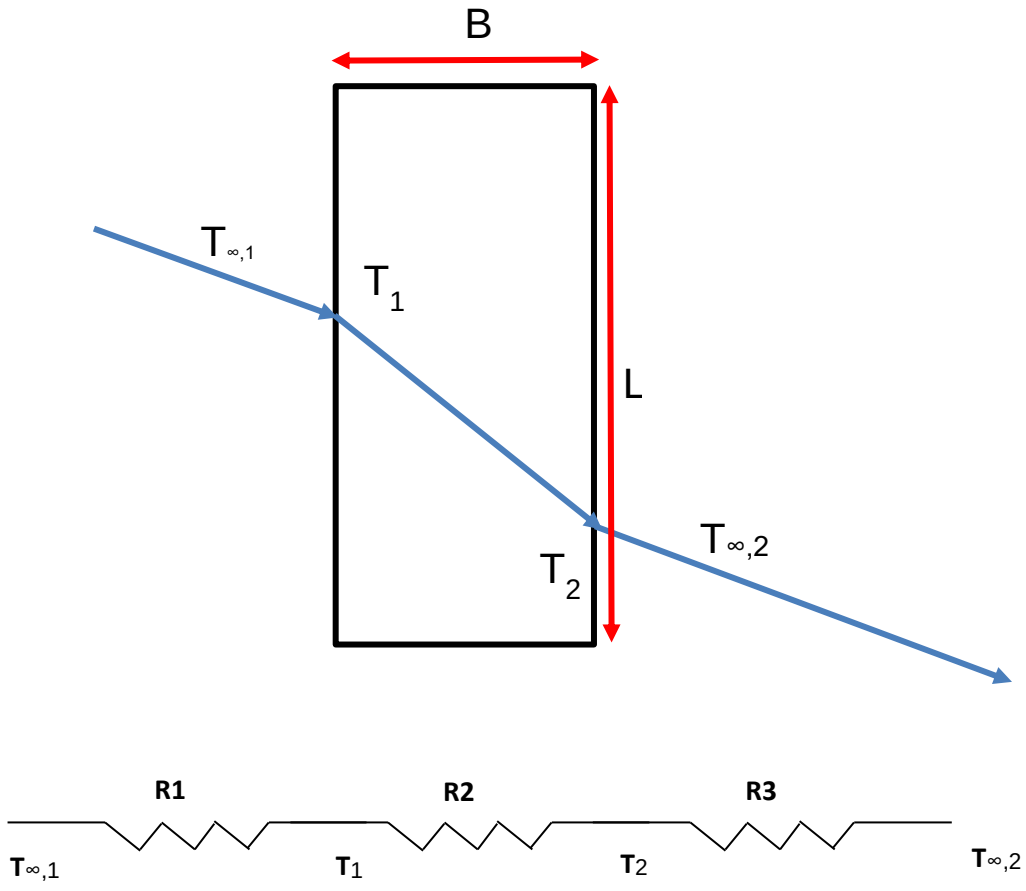

Figure 2.6 Thermal Resistance Model for composite wall

After simplification, the equation can be written as

$$q = UA\Delta T \qquad \text{(Equation 23)}$$

Where, U = overall heat transfer coefficient

Thermal resistance in cylindrical coordinate system**:**

The same concept is applied for cylindrical system. As shown in Figure 2.7, the heat transfer rate equation using thermal resistance for multi-layer radial system can be expressed as

$$q = \frac{T_s - T_\infty}{\frac{1}{2r_1\pi L h_i} + \frac{\ln(\frac{r_2}{r_1})}{2\pi L k_A} + \frac{\ln(\frac{r_3}{r_2})}{2\pi L k_B} + \frac{\ln(\frac{r_4}{r_3})}{2\pi L k_C} + \frac{\ln(\frac{r_3}{r_2})}{2r_1\pi L h_o}} \quad \text{(Equation 24)}$$

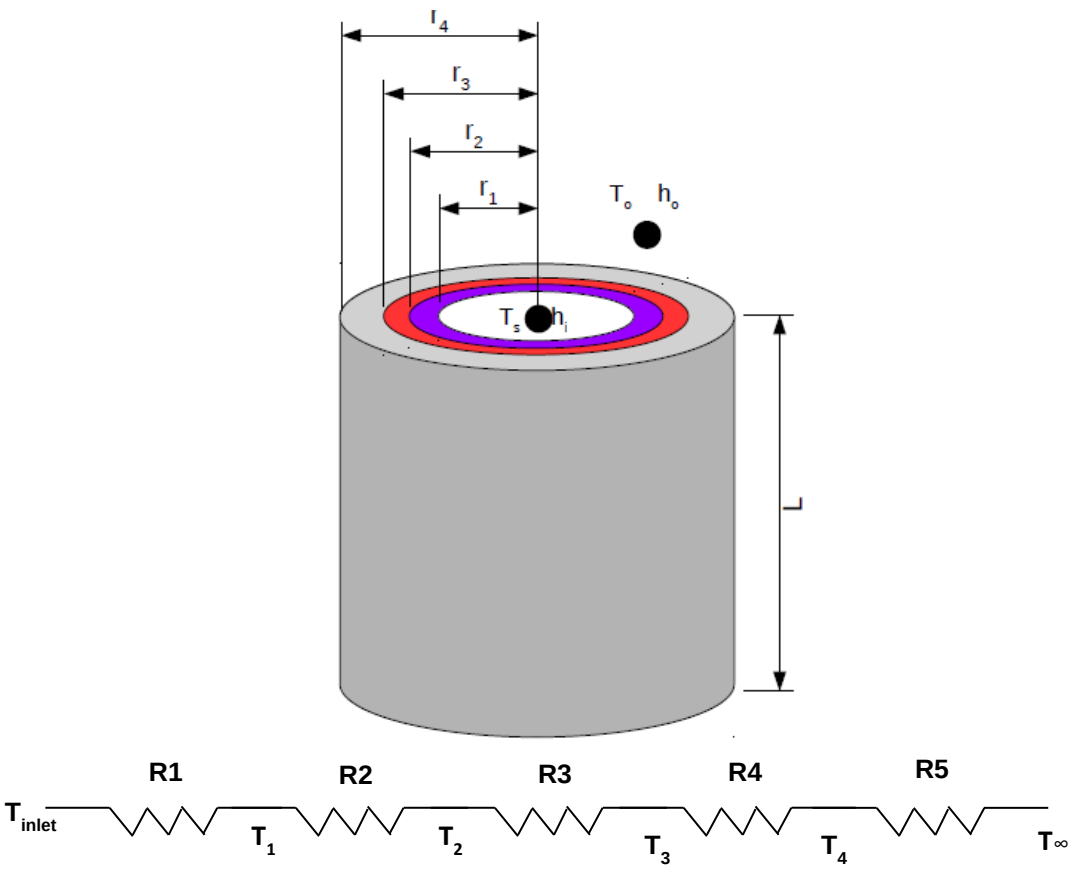

Figure 2.7 Thermal resistance model for cylindrical pipe

Heat transfer coefficient through a pipe wall**:**

The equation of the heat transfer coefficient through a pipe wall can be written as

$$h = \frac{2k}{d_i \ln \frac{d_o}{d_i}} \qquad \text{(Equation 25)}$$

where, d_o and d_i are outer and inner diameter of the pipe.

Laminar and Turbulent Flow**:**

In convection heat transfer, boundary layer plays an important role. The boundary is divided by two condition, Laminar flow and turbulent flow. The existence of these two conditions depend on surface friction and convection transfer rate.

In laminar flow, fluid follows a regular pattern. Laminar flow is also recognized as a streamline flow where the fluid velocity, pressure and other fluid properties remain constant.

In turbulent flow, fluid motion is highly irregular and is categorized by velocity momentum. In turbulent flow fluid velocity changes continuously in magnitude and direction.

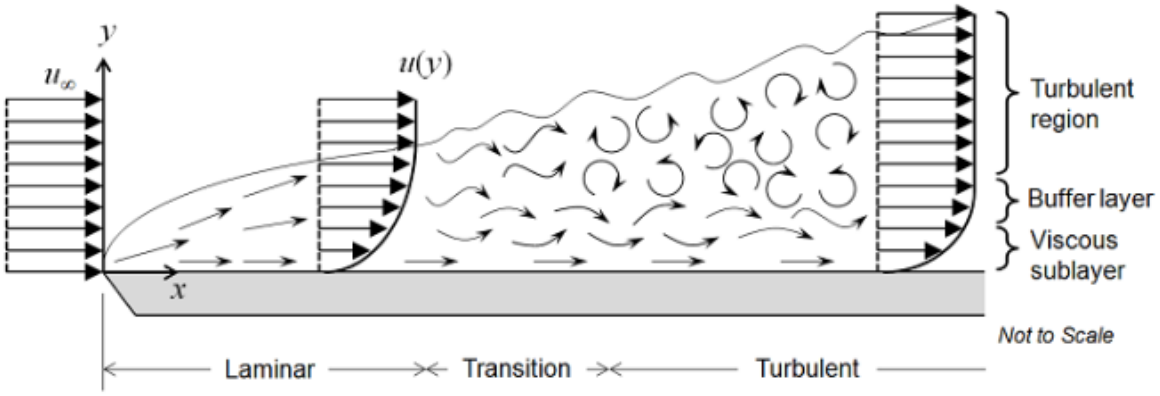

Figure 2.8 Velocity boundary layer development on a flat plate
(Bani-Hani, & Assad, 2018)

To determine boundary layer behavior, it is important to know the correlation of Reynolds number. Reynold number is a dimensionless parameter which delineate whether the fully

developed flow is laminar or turbulent.

When fluid flows through flat plate the Reynolds number can be described as

$$R_e = \rho\, u_\infty\, x/\mu \qquad \text{(Equation 26)}$$

Where, ρ = Density of the fluid (kg /m^3)

μ= dynamic viscosity of the fluid (kg /m.s)

u_∞ = Fluid Speed (m/s)

x = Location of Critical Reynolds Number

The Reynolds number can vary from 10^5 to 3 x 10^6 depending on surface roughness and turbulence level of the stream when smooth and flat plate transition occur. Typical R_e value of transition is $5x10^5$.

The convection transfer equation

In bulk movement of the fluid velocity, temperature and concentration gradients must act in accordance with several fundamental laws of nature. For the steady, two-dimensional flow of an incompressible fluid with constant properties, the continuity equation, x-momentum equation and energy equation can be described as

$$\frac{\partial u}{\partial x}+\frac{\partial v}{\partial y}=0 \qquad \text{(Equation 27)}$$

$$u\frac{\partial y}{\partial x}+v\frac{\partial y}{\partial y}=-\frac{1}{\rho}\frac{dp_\infty}{dX}+v\frac{\partial^2 u}{\partial y^2} \qquad \text{(Equation 28)}$$

Here, the right-hand side is termed as momentum flux, the first term of the right- hand side is known as pressure force and the last term of the right- hand side is known as viscous shear force.

$$u\frac{\partial T}{\partial x}+v\frac{\partial T}{\partial y}=\alpha\frac{\partial^2 T}{\partial y^2}+\frac{v}{c_p}\frac{\partial^2 u}{\partial y^2} \quad \text{(Equation 29)}$$

Here, the right-hand side is termed as c_p energy flux, the first term of the right- hand side is known as y-conduction and the last term of the right- hand side is known as viscous dissipation.

Convective Heat transfer coefficient

Convective heat transfer coefficient is a very important parameter in heat transfer mechanism. As we discussed earlier, heat transfer coefficient is directly proportional to the temperature gradient. When surface temperature is not equal to the ambient temperature, then, according to the newton's law of cooling, the local heat flux q" may be described as,

$$q''=h(T_S - T_\infty) \quad \text{(Equation 30)}$$

Here, h is the local heat transfer coefficient because flow condition varies at each point on the surface and as a result both q" and h also change along the surface.

To estimate the average convection coefficient ($h_{average}$) for the entire surface, the total heat transfer rate may be defined as

$$q=h_{average}\,A_s(T_s-T_\infty) \quad \text{(Equation 31)}$$

Where, A_s = surface area in m^2

The correlation between local heat transfer and average heat transfer coefficient can be expressed as,

$$h_{average}=1/A_s \int A_s\, h\, dA_s \quad \text{(Equation 32)}$$

There are many ways to calculate the heat transfer coefficient depending on different heat transfer mode, different fluids, flow regimes and different thermo hydraulic condition. The heat transfer coefficient is often calculated from the Nusselt number. Nusselt number (Nu) is a dimensionless parameter which is defined as the ratio of convective to conductive heat transfer across (dimensionless surface temperature gradient).

The expression of the Nusselt number can be written as

N_u = (Convective Heat Transfer)/(Conductive Heat transfer)

$$N_u = h/(K_f/L) = h\,L/K_f \qquad \text{(Equation 33)}$$

Where, h is the convective heat transfer coefficient (w/m^2k)

K_f = thermal conductivity of fluid (W/m.k)

L = characteristic length (m)

Convective heat transfer correlation There are many correlations that have been developed by many authors to determine the hate transfer coefficient in different cases such as natural convection, forced convection for internal flow and forced convection for external flow. These correlations can be used based on flow geometry and flow conditions. Since the properties of fluid are mainly temperature dependent, they can be estimated by film temperature, (Tf) is the average of surface temperature (Ts) and bulk temperature ($T\infty$).

$$T_f = (T_s + T_\infty)/2 \qquad \text{(Equation 34)}$$

For external flow, Flat plate parallel flow (Forced Convection)

$N_u = 0.664R_e^{1/2} P_r^{(1/3)}$, when $P_r \geq 0.6$ (Laminar Flow) (Equation 35)

$N_u = 0.029Re^{4/5} Pr^{1/3}$, when $0.6 < P_r < 60$ (Turbulent Flow) (Equation 36)

$N_u = 0.037R_e^{4/5}\text{-}871\ Pr^{1/3}$, when $0.6<Pr<60$, $5X10^5<Re \leq 10^8$ (Equation 37)

(Mixed boundary condition)

Here, P_r is known as Prandtl number, which is defined as the ratio of the momentum diffusivity to thermal diffusivity. The correlation of the Prandtl number can be expressed as

$$P_r = (C_p\ \mu)/K \quad \text{(Equation 38)}$$

Where,

C_p = Specific Heat (j/(kg.k))

μ = Dynamic Viscosity (N.s/m2)

K = Thermal conductivity (W/m.k)

R_e = Reynolds Number

For external flow, Cylindrical cross flow,

$$N_u = 0.3+(0.62R_e^{1/2}P_r^{1/3})/[1+(0.4/P_r)^{2/3}]^{1/4}[1+(R_e/282000)^{5/8}]^{4/5} \quad \text{(Equation 39)}$$

For internal flow, circular tubes, Laminar Flow

$N_u = 1.86((R_e\ P_r)/(L/D))^{1/3}\ (\mu/\mu_s)^{0.14}$, When T_s is constant (Equation 40)

$0.48 < P_r < 16{,}700$

$0.0044 < \mu/\mu_s < 9.75$

For internal flow, circular tubes, Turbulent Flow

$$N_u = 0.027 R_e^{4/5} P_r^{1/3} \mu/\mu_s^{0.14} \text{ when, } 0.7 < P_r < 16{,}700 \qquad \text{(Equation 41)}$$

$$R_e \geq 10{,}000$$

$$L/D \geq 10$$

Similarly, for natural convection, there is some correlation to estimate the heat transfer coefficient. In this condition, the heat transfer coefficient can be calculated from the Rayleigh Number (RaL) and Grashof Number (Gr). However, since forced convection dominates the study conditions, free convection is not discussed in detail in this chapter.

2.3 Previously Developed Numerical Models

Various researchers worked on the heat transfer mechanism for bridge snow melting systems and developed models. The literature reviewed can be sub-divided into two broad categories: Steady-state models and Transient models.

Steady State Models

Steady state models assume the temperature of the system is independent of time. In these models, the heat source (heated fluid in embedded pipes) and the heat sink conditions (ambient temperature, wind speed, convection coefficient etc.) are assumed constant. Hence, chronological variations in the system are not accounted in these models.

A one-dimensional steady state analysis of hydronic snow melting system was proposed by Chapman et al. (1952). He proposed that the heat output and eventually the performance of a snow melting system depended on the interaction of five independent variables: heat of fusion, heat for increasing the snow temperature to melting point, heat of vaporization, heat transfer by convection and radiation, and heat loss to the ground. The accumulated snow acts as an insulation against heat loss and evaporation at the surface boundary. To account for this effect, Chapman (1957) introduced a dimensionless snow free area ratio (A_r), which is the ratio of effective snow

free area to the total surface area. The heat output at the surface for melting snow was derived to be

$$q_0 = q_s + q_m + A_r q_h + q_e \quad \text{(Equation 42)}$$

$$q_s = \rho s c_j (t_f - t_a) \quad \text{(Equation 43)}$$

$$q_m = \rho s h_{if} \quad \text{(Equation 44)}$$

$$q_e = (aV+b)(P_{wv} - P_{av}) h_{fg} \quad \text{(Equation 45)}$$

$$q_h = c(aV+b)(t_f - t_a) \quad \text{(Equation 46)}$$

Where, q_0 = Total required heat flux, Btu/hr-ft^3 (W/m^3)

q_s = Sensible heat flux to raise temperature of the snow from that of the air to the melting point, Btu/hr-ft^3 (W/m^3)

A_r = Equivalent snow-free area ratio, dimensionless

q_m = Latent heat flux for melting snow, Btu/hr-ft^3 (W/m^2)

q_h = Combined convective and radiative heat flux, Btu/hr-ft^3 (W/m^2)

q_e = Heat flux for evaporating water on the surface, Btu/hr-ft^3 (W/m^2)

ρ = Density of liquid water, 5.2 lb/ft^2-in or 1.0 kg/m^2-mm

s = Snowfall rate water equivalent, inches/hr (mm/s)

c_i = Specific heat of ice, 0.5Btu/lb-ºF or 2100 J/kg-ºC

t_f = Water film temperature, ºF (ºC)

t_a = Ambient temperature, ºF (ºC)

h_{if} = Heat of Fusion, 143.4 Btu/lb or 3.3 x 10^5 J/kg

a = constant, 0.0201 hr^2/mile-ft or 530.84 s^2/m^2

b = constant, 0.055 hr/ft or 649.61 s/m

V = Wind speed, mph (m/s)

P_{av} = Partial pressure of water vapor in ambient air, in. Hg (Pa)

P_{wv} = Partial pressure of water vapor in saturated air film on surface,

in. Hg (Pa)

h_{fg} = Heat of vaporization of water, Btu/lb (J/kg)

c = Constant, 11.4 Btu/hr^2- ft - ºF or 0.005476 W/m-s-K

However, the model assumed uniform film temperature throughout the surface and ignored the spatial distribution of temperature and intensity of heat due to heating element locations.

A two-dimensional finite difference steady-state model was developed by Schnurr & Rogers (1970) for a hydronically-heated slab. This model assumed uniform temperature at the pipe surface and a snow free surface. To incorporate the variation of surface temperature, the solution domain was limited to ½ of the pipe spacing, assuming minor temperature difference between adjacent pipes. Repeated iterations are required to determine discrete surface conditions to maintain the required surface conditions for melting snow. However, this model had certain limitations as it assumed only snow free surfaces.

Kilkis (1994) proposed a simplified model that allowed quantification of snow cover on the surface. Convection and radiation losses were estimated with an empirical correlation proposed by Williams (1976) and Williams (1967) respectively.

$$q_e=(aV+b)(t_f - t_a) \qquad \text{(Equation 47)}$$

Where, a = constant, 0.14 Btu/mile-ft^2-ºF or 1.78 J/m^3-ºC

b = constant, 0.39 Btu/hr-ft^2-ºF or 2.21 W/m^2-ºC

This simplified model allows incorporating pipe layout, weather conditions and snow cover into snow melting performance determination. Using this model, the required fluid temperature and range of surface temperature of the slab could be determined to assess the snow melting performance. However, since this is a steady-state model, the time dependent weather variations

could not be predicted with this model.

Steady state models provide a stand-alone representation of slab thermal behavior within a single time step. The dynamic and chronological changes in weather conditions and response of the heated slab cannot be predicted with a steady-state model. Also, steady-state models assume instantaneous heat transfer from the heated pipe to the slab surface, which is idealistic. Hence, transient models are essential to simulate the variations in weather conditions, response of the slab and snow melting performance in real time.

Transient Models**:**

Transient models address the major shortcoming of steady-state models, considering the time dependent variations of weather conditions and heat flux. Most of the literature reviewed on transient models relied upon the basic steady state model developed by Schnurr & Rogers (1970). The intent of the study of these models is to review the concepts built into these models and hence, the mathematical equations and their theoretical interpretations have not been discussed in detail for the scope of this study. A summary of reviewed two-dimensional transient model during this study is presented below:

Leal & Miller (1972) worked on the model developed by Schnurr & Rogers (1970) and included the heat conduction variations in the slab in their model. The heat balance at the surface boundary was calculated using the equation proposed by Chapman (1952). The bottom boundary of the slab is assumed adiabatic. However, a critical assumption of the proposed finite difference model is the linear relationship between temperature and heat flux at the slab surface exposed to ambient temperature. Since the slab surface is exposed to snow melting where a phase change occurs, the assumption of linear relationship between heat flux and temperature is impractical.

Schnurr & Falk (1973) extended the Schnurr & Rogers (1970) model by implementing a finite difference model with transient heat transfer through conduction. The bottom boundary was assumed adiabatic and the equation proposed by Chapman (1952) was used to estimate the heat output at the top boundary. The shortcoming of this model was that it did not allow snow accumulation on slab surface, as it assumed system activation before snowfall start and hence,

immediate snow melting on the heated slab surface. This idealistic assumption prevented realistic performance assessment as it ignored the insulation effect when the slab was covered with snow. Also, constant weather conditions are used, which is unrealistic. Dynamic changes in weather conditions and slab temperature are critical parameters to assess snow melting performance of the system.

Chiasson, Spitler, Rees & Smith (2000) proposed a model similar to Schnurr & Falk (1973), with a different method to calculate heat flux at the top surface boundary. Following are the main conceptual features of the model:

i) Solar radiation was added as a variable in the heat output at the top surface

ii) Convective heat flux and radiative heat flux were analyzed separately

iii) Convective heat transfer coefficient taken as maximum of free and forced convection coefficients.

iv) Pipe wall boundary condition was not uniform and rather was specified as a heat flux variable. This variable depended on the convective heat transfer from the heated liquid from the pipe.

Although this model had significant improvements from the previous models, it had certain shortcomings:

i) Insulating effect of snow was not accounted as snow was treated as ice on the surface.

ii) Model was validated under slab dry conditions and not under snow melting conditions.

Rees, Spitler, & Xiao (2002) developed a two-dimensional transient model for analyzing hydronic heating system performance. The proposed model was a boundary fitted coordinate finite volume model, with solution domain like previous models. The dynamic effects of weather and slab response can be analyzed using this model. Constant heat flux must be specified as the boundary condition at the pipe surface. Solar radiation was not accounted for in this model. However, this model was a significant improvement over all the previously discussed models, as it had provisions to represent seven different surface conditions at the slab surface. A description

of the possible surface conditions allowed by the model are provided below:

i) Dry: Slab surface free from moisture (liquid and ice), irrespective of surface temperature

ii) Wet: Surface above freezing and has retained liquid, but with no ice deposit

iii) Dry Snow: Surface temperature below freezing, no concurrent melting, with fresh deposit of snow on the surface

iv) Slush: Surface is at freezing point and contains snow crystals fully saturated with water.

v) Snow and Slush: Surface is at freezing point. Surface contains partially melted snow (upper portion is dry snow and lower portion is ice saturated with water)

vi) Solid Ice: Surface temperature is below freezing point and solid ice on surface (no pore water).

vii) Solid Ice and water: Surface temperature at freezing point. Solid ice and water on surface, potentially due to melting snow or surcharge rain.

The mass and energy balance in snow and/or slush layers must be simultaneously solved, which requires nested iterations, requiring immense computational effort. Although the model may be helpful to analyze a short storm event, a performance assessment involving several years' worth of weather variables may be excessively computationally intensive to be of practical significance.

Determining Heating Capacity of Snow Melting Systems

The energy balance equation proposed by Chapman (1952, 1957) shows the variables involved in the heating capacity of the snow melting system and the resultant output. He suggested that the design parameters should be based upon the frequency distribution of heat requirement rather than selecting the individual design variables (snowfall rate, ambient temperature, wind speed etc.). The intent of the design should be selecting a capacity for a pre-determined number of annual snowfall hours based upon actual hourly load and frequency distribution. Chapman (1957) also proposed a classification system to measure snow-melting performance as described below:

- Class 1 (Residential): The entire surface is allowed to be covered with snow during snowfall ($A_r = 0$). The system should melt the accumulated snow after the snowfall event.
- Class 2 (Commercial): 50% of the surface is allowed to be covered with snow ($A_r = 0.5$).
- Class 3 (Industrial): Entire surface free of snow during snowfall ($A_r = 1$)

A study by Williams (1973) proposed equations for estimating heating requirements based on snow melting tests over three years of winter in Ottawa, Canada. Based on the experiments, he concluded that it requires more heat to maintain an ice-free surface after the snowstorm than during a snowstorm. Therefore, calculating rate of surface heat loss from the ice-free pavement based on the weather data of the storm will help to estimate of heating requirement for the system. He also suggested that the heat transfer coefficient should be modified based on the spatial conditions of the system, such as exposure to the wind, wind speed measurement height and size of the heated area.

A simplified design heat requirement approach was proposed by Kilkis (1994a). He proposed the following equations:

$$t_c = t_b + \frac{(t_{ref} - t_b)}{(0.1 + 1.2\, C_{performance})} \qquad \text{(Equation 48)}$$

$$s = \left(\frac{SF}{24}\, C\right)\frac{\rho_s}{\rho_w} \qquad \text{(Equation 49)}$$

Where, t_c = snowfall coincident design air temperature, º F or º C

t_b = design outdoor temperature, º F or º C

t_{ref} = Reference Temperature, 33º F or 0.56º C

$C_{performance}$ = Snow Melting Performance class (1, 2 or 3 corresponding to snow melting performance class described before)

The heating requirement for all the phases of the system operation (before snowfall, during snowfall and after snowfall) were calculated with the previously discussed steady state model proposed by the same author (Kilkis, 1994b). From the three heating requirements obtained, the

maximum was chosen as the design heat requirement.

The ASHRAE RP-926 report concluded that there was no simplified approach to accurately estimate the design heating requirement of the snow melting systems based on limited meteorological data (Ramsey, Hewett, Kuehn, & Petersen, 1999; Liu, 2005). Consequently, the ASHRAE Handbook – HVAC Applications (1999) followed frequency analysis method proposed by Chapman (1952, 1957). Spitler, Rees, & Liu (2001) concluded that the heating load requirement calculated using the transient model were several times higher than the ones calculated using steady-state models for maintaining the same surface conditions, This is because the steady-state models do not consider the dynamic changes in weather and slab conditions during the storm.

Liu (2005) considered the drawbacks of the previously discussed models. He identified that modeling of hydronic heat system must be a transient model to account for variations of physical properties of snow, weather conditions during the storm event. He also suggested that a successful model requires consideration of phase change during the snow melting process as shown below:

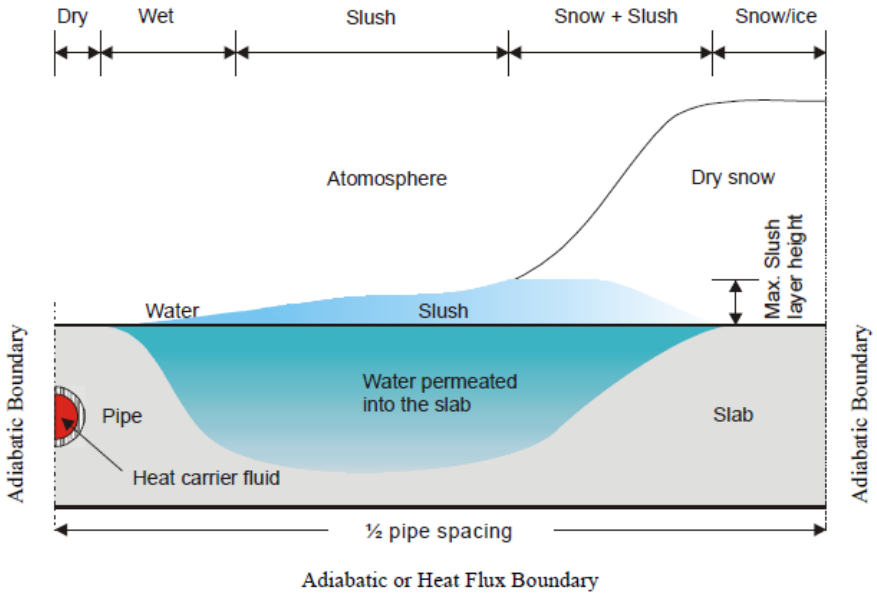

Figure 2.9 Phase change during snow melting process (Liu,2005)

Liu (2005) also proposed that modeling of a snow melting system should consider prior condition of the surface and its heat flux to accurately determine the current conditions. For example, snow falling on a dry pavement with temperature below freezing point will not lead to any melting. However, if the same slab existed at the freezing point or higher, instantaneous snow melting may occur as the snow falls on the surface. He adopted the surface classification system proposed by Rees, Spitler, & Xiao (2002), described below in Table 2.2:

Table 2.2 Surface Classification System (Rees, Spitler, & Xiao, 2002; Liu, 2005)

Surface Condition	Definition
Hoarfrost	Pavement surface temperature shall be below freezing. Surface is covered with frost due to sublimation of water vapor with ambient air on a cold surface
Dry	Pavement surface temperature may be above or below freezing. Surface temperature may be above or below freezing
Wet	Surface temperature is above freezing. Surface has some liquid water retained on it, but is free of ice.
Dry Snow	Surface temperature is below freezing point, so no concurrent snow melting. Hence, surface is covered with dry snow without any liquid.
Slush only	Surface temperature is at freezing point. Surface contains ice crystals fully saturated with water.
Snow and Slush	Surface temperature is at freezing point. The surface contains partially melted snow (lower part saturated with water, upper part dry snow)
Solid ice	Surface temperature must be below freezing point. Pavement covered with solid ice without pores like snow.

An important consideration in the model development by Liu (2005) is distinguishing the "Slush only" condition from "Slush and snow" condition. A schematic representation of heat transfer

in both models are shown below:

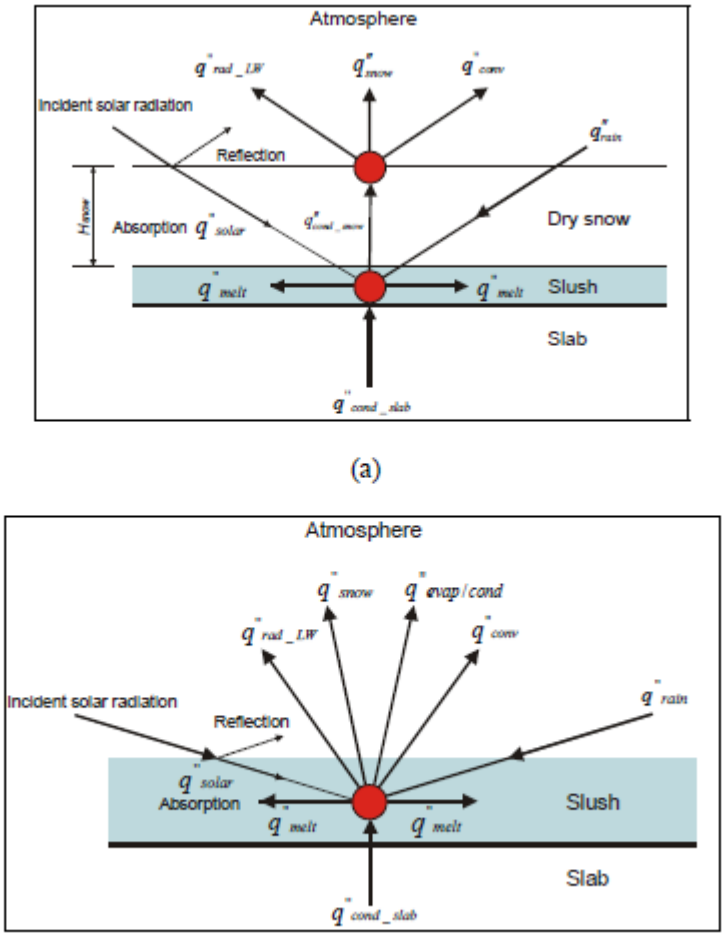

Figure 2.10 Schematic representation of heat transfer in (a) two-node “snow and slush” model, (b) one-node “slush only” model (Liu,2005)

Considering the seven possible surface conditions, the difference in their heat transfer mechanisms and their chronological order and possibilities, Liu (2005) developed his model based on the following algorithm:

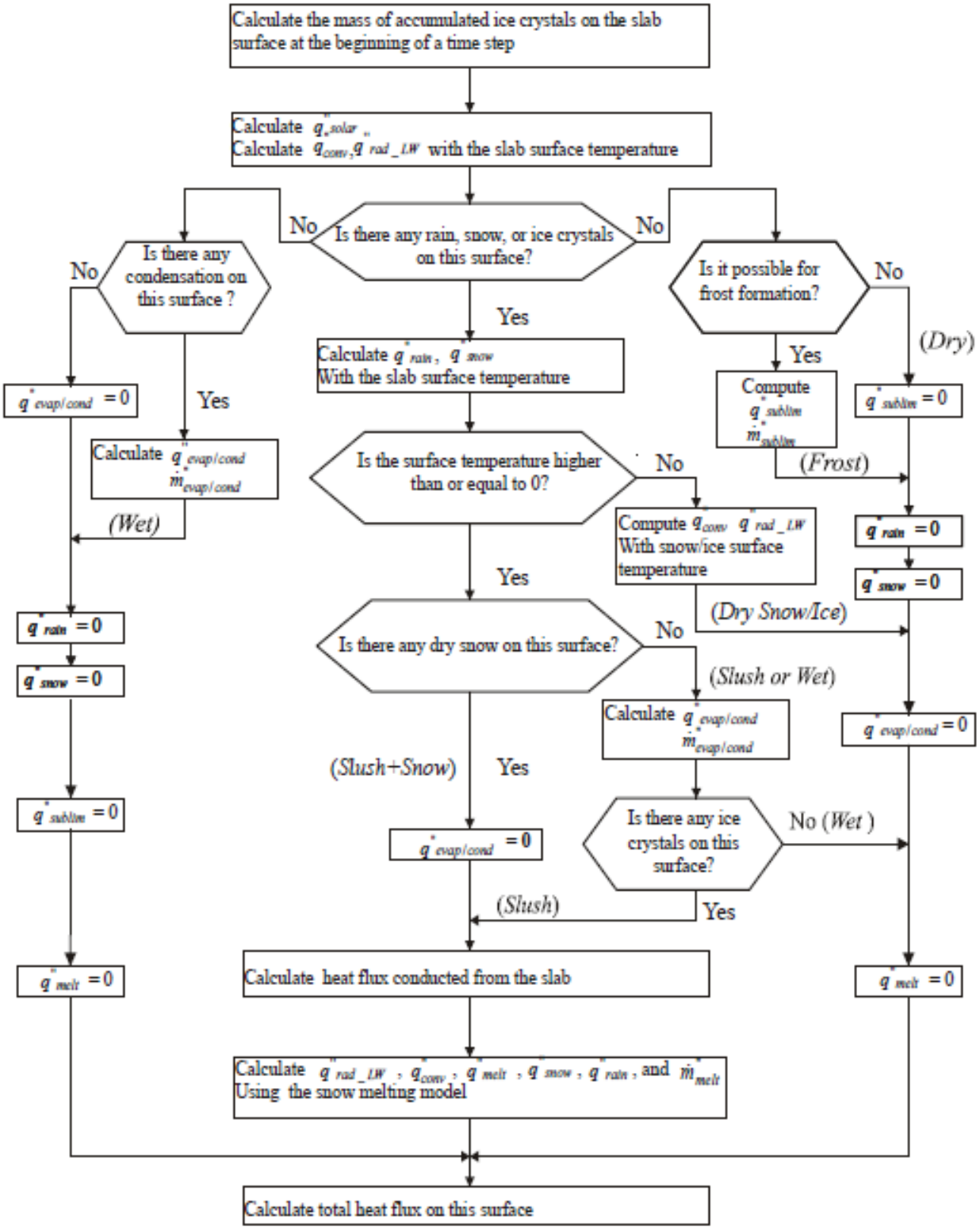

Figure 2.11 Algorithm of snow melting model development (Liu,2005)

Each surface condition is evaluated with their specific heat transfer mechanisms and an appropriate set of heat and mass balance equations proposed for it. Solution of these equations involve successive substitution to determine the node temperatures, melting temperatures, melting rate and current mass of ice.

The model was validated through an experimental hydronic snow melting system installed in a bridge at Oklahoma State University (Liu, 2005). The experimental bridge deck was 60 feet long and 20 feet in width. The hydronic melting system installed consisted of ¾" diameter cross-linked polyethylene pipe, at 3.5-inch depth spaced at 1 feet center-to-center spacing. An Aqueous solution of propylene glycol (39% by mass) was used as a heat carrier fluid. The maximum possible fluid temperature is set to 130ºF and the system was set to maintain an average bridge surface temperature of 40ºF during a potential snowfall. The prediction of the developed model was validated with the corresponding measure data of the experimental bridge setup.

However, the surface conditions considered in this model were one-dimensional and can predict only the average bridge surface temperature. Liu (2005) recommends development of a three-dimensional model to account for spatial variations, especially for evaluate heat and mass transfer phenomena occurring at the edges of the heated slab. Also, following the ASHRAE RP-926 report recommendations, there is no simplified approach to accurately estimate the design heating requirement of the snow melting systems with limited meteorological data. Additionally, all the above discussed models were proposed for an internal hydronic system. There is no systematic literature available to understand the behavior of externally installed hydronic system. Hence, development of a three-dimensional numerical model is required to develop a holistic understanding of bridge snow melting system performance in the DFW Area.

Chapter 3.
EXPERIMENTAL PROGRAM

3.1 Introduction

To estimate the efficiency of a geothermally driven de-icing system, implementation of an experimental model in the field is required. Hence, Hurley (2019) and the geothermal research team under Dr. Yu conceptualized an experimental program to understand the efficiency of the de-icing system. A small scaled model, 1.83 m x 1.22 m x 0.1 m (6’ x 4’ x 4”) concrete slab was set up outdoors to replicate the actual weather conditions and assess the de-icing of bridge overpasses with geothermal energy. The step-by-step experimental set up is explained in the following sections.

3.2 Slab Setup

A conventionally reinforced concrete slab (1.83 m x 1.22 m x 0.1 m) was supported on concrete blocks on both ends. The slab was confined along the East-West Direction by a cubicle and Civil Engineering Laboratory Building (CELB). After securing the slab in place, PEX pipes were installed at the base of the slab. The pipes were installed in a meandering fashion, in a series of 9 loops spaced 0.15 m (6”) apart (Figure 3.1). The pipe setup was then encased with a 0.05 m (2”) thick wooden framework to enable application of insulating foam (Figure 3.2).

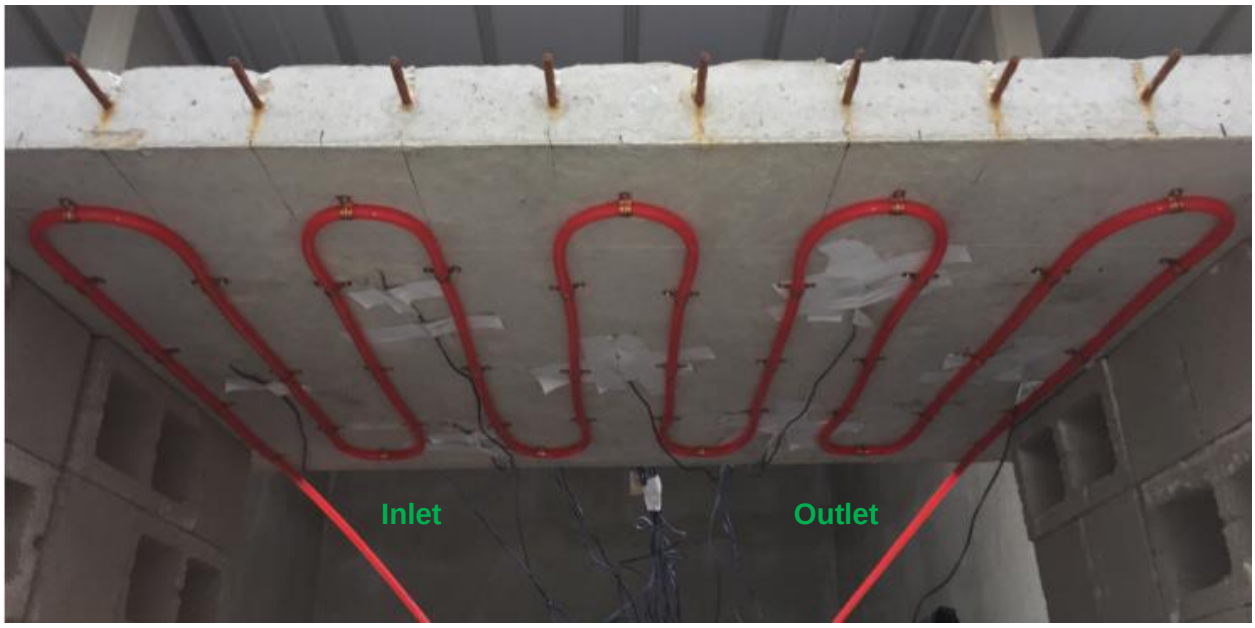

Figure 3.1 Slab Setup and PEX Pipe Arrangement

Figure 3.2 Wooden Framework Perimeter around PEX Pipes

3.3 Thermocouple Installation

To determine the spatial distribution of heat in the slab, thermocouples were required at different locations within the slab. Type T thermocouples were chosen because of the expected lower temperature usage for the study. Type T thermocouples were drilled into the slab at planned location and depths to capture the spatial heat variations within the slab. Figure 3.3 shows the location plan of the thermocouple setup, with the depths in parentheses. The depths shown in figure are with respect to the top of the slab. For example, thermocouple location T-4 has four Type-T thermocouples at different depths within the slab. The top thermocouple is located 0.013 m (0.5”) from the top surface of the slab, whereas the bottom thermocouple is located 0.089 m (3.5”) from the top of the slab.

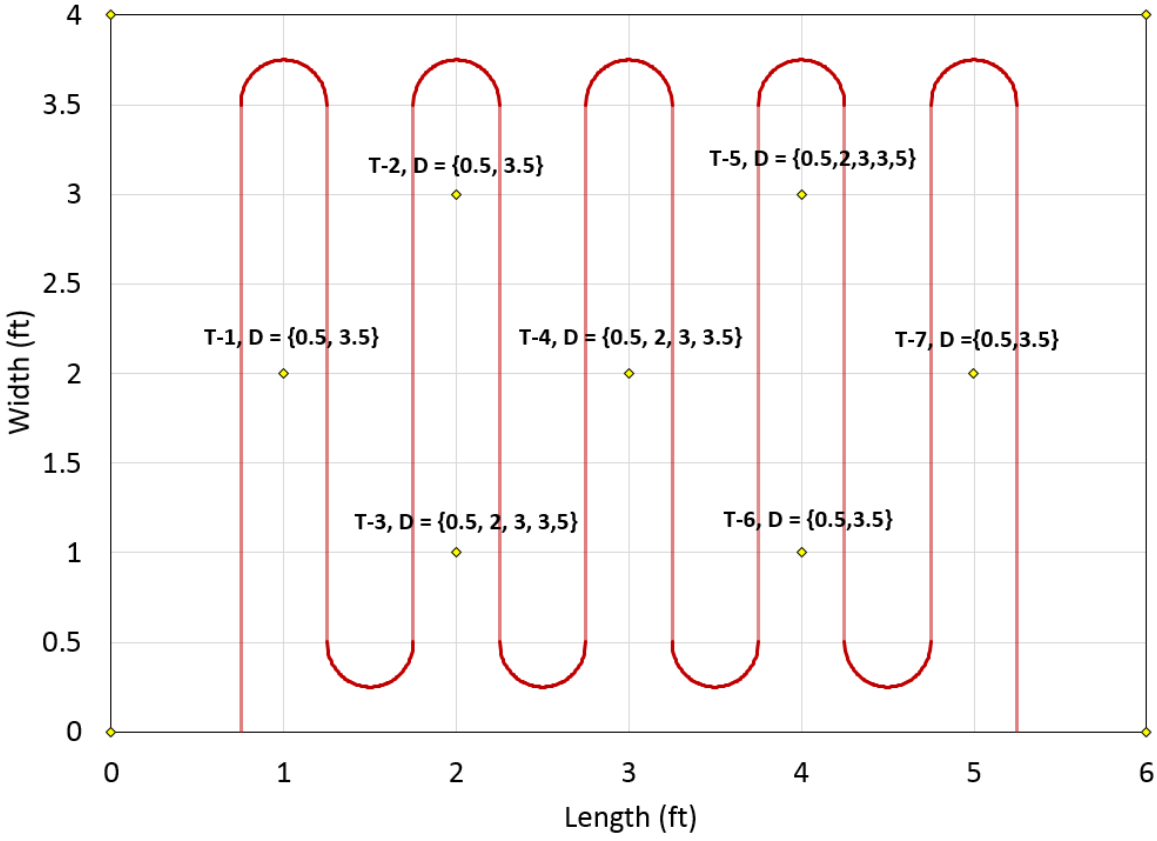

Figure 3.3 Thermocouple Location Plan

3.4 Insulation installation at the bottom

Closed cell spray foam was used as the insulating material to prevent heat loss at the bottom of the slab. An insulating layer at the slab base would maximize the amount of heat available to the top surface for de-icing, and hence, maximize the efficiency of the system. Closed cell spray foam was chosen due to its denser, more durable and better heat insulating properties than open cell foam with same thickness. The foam was sprayed within the enclosed 2-inch-thick wooden framework with 0.5-inch-thick PEX pipe (Figure 3.4). Hence, the minimum and maximum thickness of the foam as 1.5 inch and 2 inches respectively. Additional insulation was provided at the inlet and outlet locations to limit external heat loss.

Figure 3.4 Closed cell spray foam application within peripheral wooden framework

3.5 Water bath installation and setup to simulate hydronic circulation

A 19-liter (5-gallon) water bath capable of maintaining approximately constant temperature was chosen to simulate the circulation system (heat pump). The water bath could circulate the hot water within a range between 10ºC (50ºF) and 82ºC (180ºF). The water bath in the experimental setup essentially simulates the heat extraction of the water from underground loops. The inlet and the outlet were connected to the water bath and circulation was performed using a water pump at approximately 7.5 liters (2 gallons) per minute. Figure 3.5 shows the setup of the system.

3.6 Experimental Program

A planned experimental program was undertaken to understand the behavior of the slab in response to the hydronic heating system installed. The experimental program undertaken is summarized in Table 3.1. Each of the experimental weather events are explained in detail in the subsequent subsections.

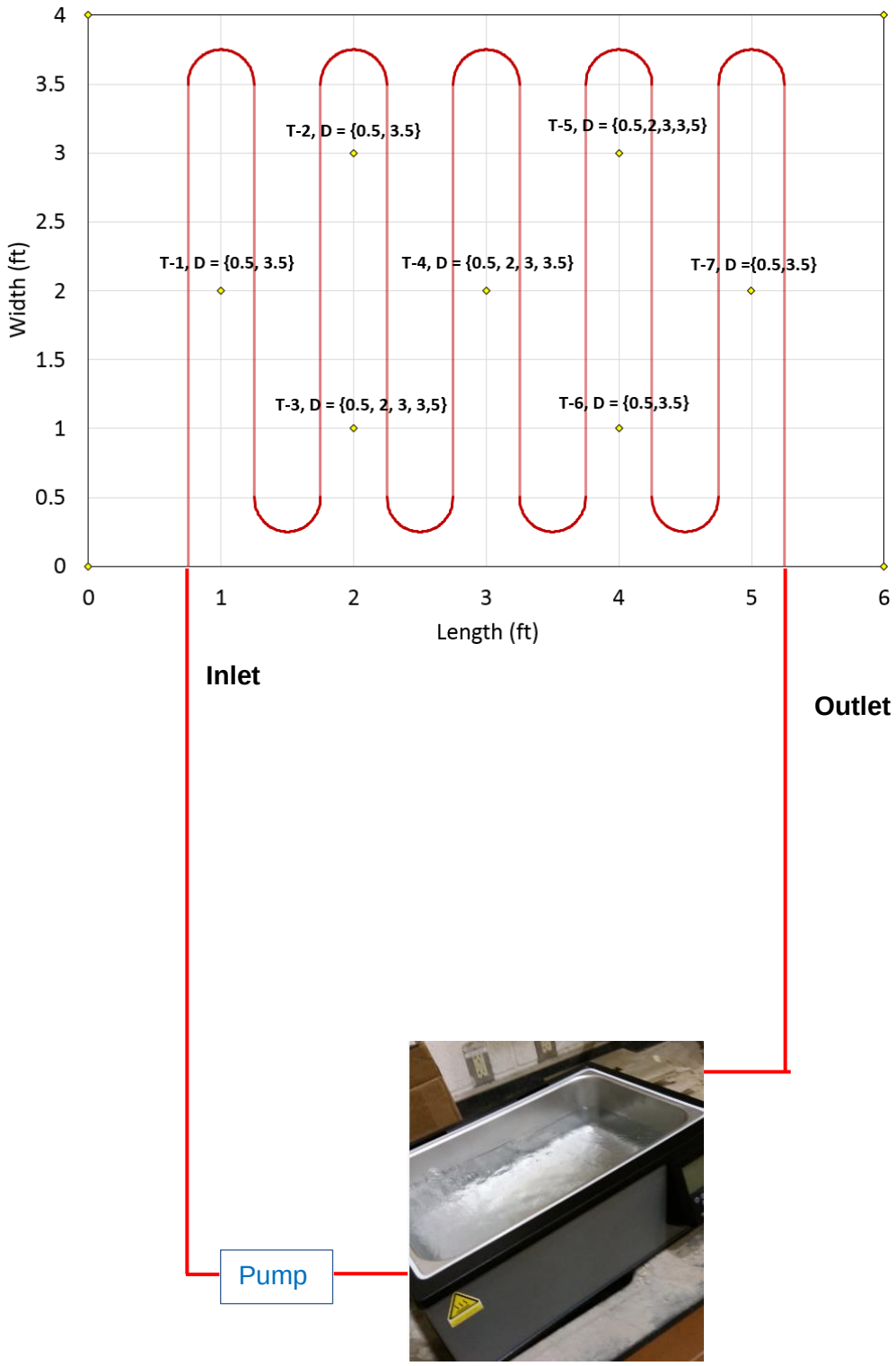

Figure 3.5 Schematic setup for the experimental program

Table 3.1 List of Events for Experimental Program

Serial No.	Date	Time	Event	Comments
APPARATUS SET-UP				
1	12/18/2018	N/A	Slab was secured on concrete blocks in open environment	Only slab installed
2	12/20/18 - 12/21/18	N/A	Thermocouples installed within slab	
3	1/4/2018	N/A	Wooden Framework constructed to conceal spray foam	Support for insulating foam installation, no insulating foam installation yet
4	1/7/2018	N/A	Water tank and pump were set-up to complete hydronic system	
5	1/8/2018	N/A	Water tank remained off while the thermocouples were initiated for the pre-test	
TEST PROGRAM				
6	1/12/18 - 1/15/18	6:36 P.M. of 01/12 to 5:41 P.M. of 01/15	Pre-Test 1	To observe the effects of weather on the thermal behavior of the slab **without external heat input**
7	1/17/18	N/A	Spray foam injected within wooden framework as insulator	
8	1/26/2018	N/A	Water tank was turned on and set to 38ºC (100ºF)	
9	2/7/2018	N/A	Water tank was set to 21ºC (70ºF)	

10	2/8/2018	N/A	Snow gun assembly	No actual test done with snow gun on the day, just assembled.
11	2/11/2018	2:34 A.M. to 10:20 A.M.	Winter Event (Snow Gun), circulating water temperature set at 22ºC (70ºF)	Performance of bridge deck under simulated snowing conditions **with external heat input**
12	2/21/2018	1:53 A.M. to 3:53 P.M.	Cold Front, circulating water temperature set at 32ºC (90ºF)	Performance of bridge deck under extreme weather conditions **with external heat input**
13	3/5/2018	N/A	Water tank moved, foam encapsulating tank loosened	

3.6.1 Pre-Test

It is essential to understand the behavior of the slab without heat input to differentiate the influence of hydronic heating system on the slab. Further, it was also necessary to determine if there was any flaws or inconsistencies in the installation before the full-scale testing was initiated. Hence, a pre-test was conducted before initiating circulation to determine how the concrete slab alone reacted in response to ambient temperature and wind speed. The pre-test was conducted after the installation of the slab and PEX pipes, but before the insulating foam was sprayed on the bottom of the slab.

As seen from Figure 3.6, the temperature within the slab follows a cyclic trend based on the daily diurnal cycle. The minimum slab temperature was observed at a time slightly later than the occurrence of the minimum daily temperature due to time lag. It takes a certain amount of time for heat to dissipate in response to a decrease in the environmental temperature, and the time is directly proportional to the depth from the surface of the slab. This trend can be attributed to the low thermal conductivity of concrete. Hence, it can be clearly seen that the slab temperature was greater than the environmental temperature for most of the nightly cycle unless a warm front occurred. Conversely, the slab temperature was observed to be lower than the environmental temperature for most of the daily cycle unless a cold front occurred.

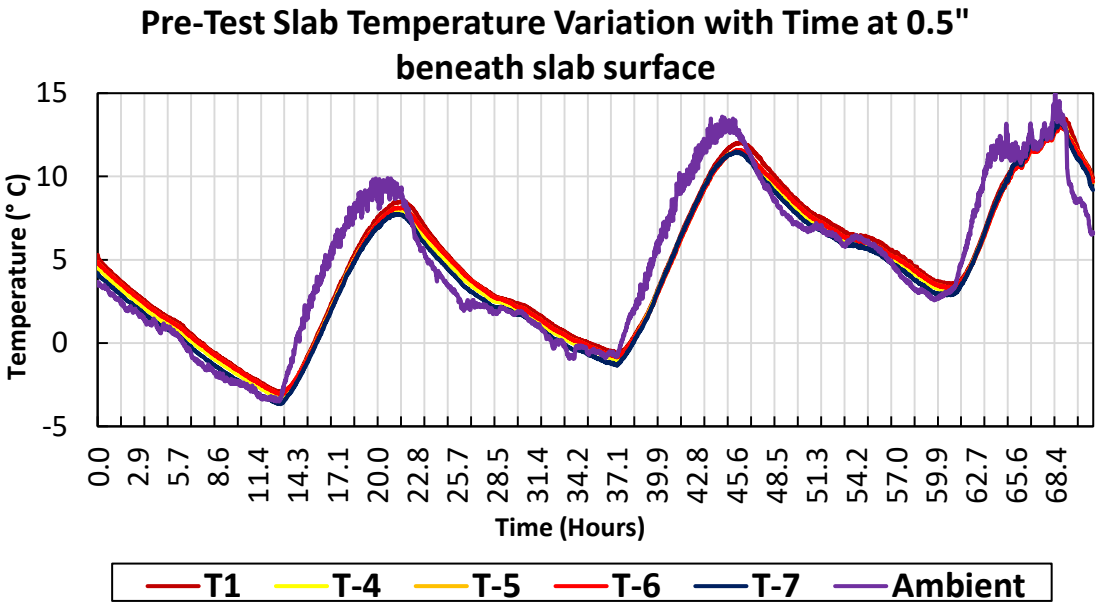

Figure 3.6 Pre-test results for installed thermocouples in the experimental deck slab

3.6.2 Winter Event

After the determination of the response of the slab without external heat input, the circulation system was turned on. The circulation temperature was set at 21ºC (70ºF). It was now required to study the efficiency of the system in response to an extreme weather event. Based on the weather forecast, 11th February was supposed to be a cold day, where the temperature was expected to drop below freezing. To simulate precipitation, a snow gun was assembled to simulate intermittent cold mist over the slab (Figure 3.7). The response of the slab was recorded with the spatial distribution of thermocouple during the entire event (Figure 3.8)

Figure 3.7 Snow gun assembly (inset) and experimental setup used during the experiment

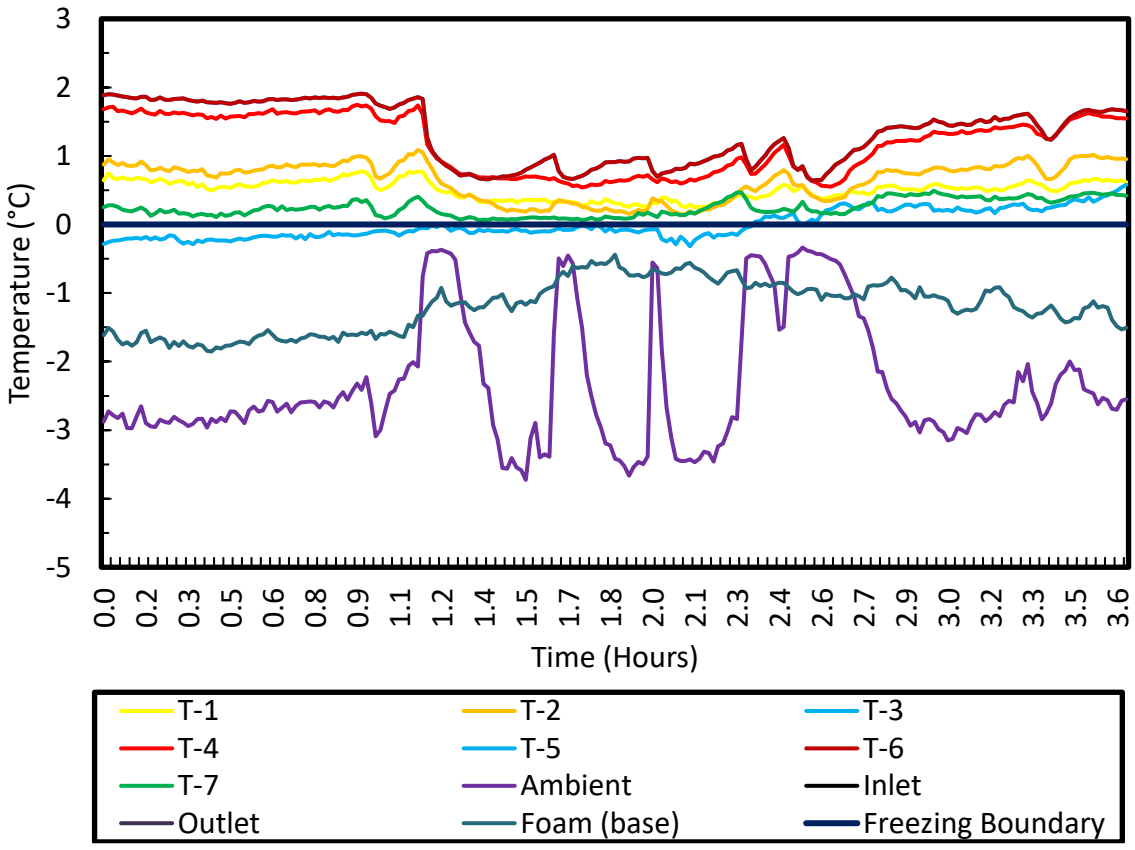

Figure 3.8 Thermocouple temperature at 0.5” depth with time during the winter simulation

From Figure 3.8, it is observed that the temperature immediately dissipated following the application of icy conditions to the slab. There was an immediate rebound in the slab temperature after the cessation of the snow gun application. Hence, each dip in environmental temperature corresponded to the cessation of the snow gun, which resulted in ice accumulation along unheated portion of slab as the environmental temperature was around - 4°C (25°F). Each thermocouple was able to maintain above freezing temperatures for the duration of the test as shown by Figure 3.8.

3.6.3 Cold Front

Since winter precipitation is uncommon in DFW area, it was necessary to study the performance of the system at temperatures below freezing, but without any precipitation. Based on the weather forecast, an experiment was set up to capture the response of the system during a cold front between 19th February 2018 and 21st February 2018. The circulation temperature was set at 32ºC (90ºF). The heat distribution patterns due to circulation and the overall efficiency of the system to maintain surface temperature above freezing were recorded, as shown in Figure 3.9.

From Figure 3.9, it is evident that the bridge deck was able to maintain temperature above freezing during the entire event. All the thermocouple locations recorded temperatures a few degrees over ambient temperature.

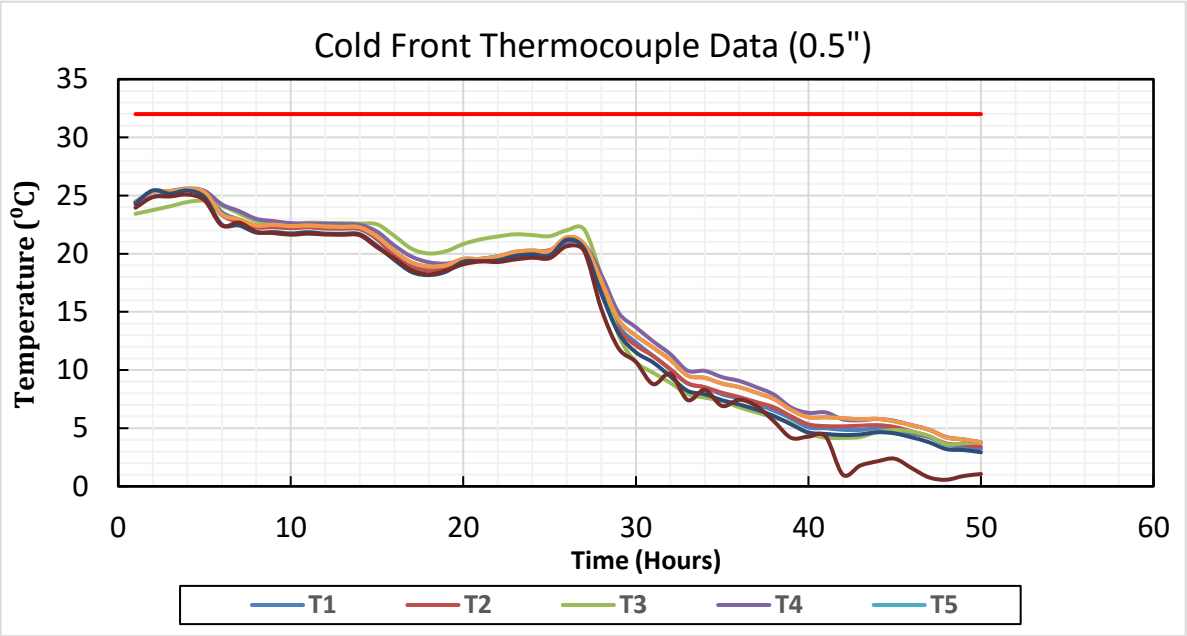

Figure 3.9 Temperature of bridge decks at different locations during Cold Front

Chapter 4.
Numerical Modeling in COMSOL

4.1 Introduction

The main objective of this study is to develop a numerical model to assess the performance of implementing hydronic heating system for de-icing of bridges in DFW area. From the literature review, it is deduced that the previously discussed hydronic system models were developed for internal hydronic system. Also, the ASHRAE RP-926 report concluded that accurate estimation of snow melting system performance is not possible with limited meteorological data. Hence, a three-dimensional numerical model is required to consider comprehensively consider the effectiveness of the proposed external hydronic heating system for de-icing of the bridges around DFW area. Hence, following are the objectives of the current research:

1) Developing a three-dimensional numerical model of proposed hydronic system using COMSOL.
2) Validation of the model data using experimental results obtained from the experimental bridge deck slab fitted with proposed hydronic heat system.
3) Compare the numerical and experimental test results with analytical test results obtained using steady-state thermal resistance modeling.

To achieve these objectives, an experimental program was first set up. A small-scale model of the bridge deck slab, 1.83 m x 1.22 m x 0.1 m (6’ x 4’ x 4”) concrete slab, was set up outside the Civil Engineering Laboratory Building (CELB) of UTA. Meandering PEX pipes were attached at the bottom of the slab and type-T thermocouples were installed at various locations and depths of the slab in the bridge to record spatial temperature distribution. The experimental setup and details are discussed in detail in Chapter 3.

A numerical model was developed using COMSOL. The efficiency of the hydronic heating system was tested during the weather events occurring for 2018 winter (January and February). The recorded temperatures from the thermocouple were analyzed to determine the spatial distribution of heat in the slab. The weather data (temperature and wind speed) were obtained

from the weather station in Dallas-Fort Worth Airport, which is located about 20 miles North-East of the test site. After a winter event, the data obtained from the experimental setup were collected. The weather data from the weather station were also obtained. The temperature and wind speed obtained from the weather station were used as inputs in the developed three-dimensional COMSOL model. Transient analysis was run on the entire period of the weather event. The outputs obtained from the model at different thermocouple locations were compared with their experimental counterpart and deviations, if any, were investigated.

Once the numerical model outputs were validated against the experimental results multiple weather events, the numerical model was used to assess the performance of the setup for historical weather conditions in Dallas-Fort Worth Area. The weather data (temperature and wind speed) for coldest days of five consecutive years (2014 to 2018) in Dallas were obtained from the DFW Airport weather station. These data were used as inputs in the numerical model with varying inlet temperature to study the effectiveness of the system at different conditions.

To understand the differences between three-dimensional numerical model and thermal resistance based analytical model, the same weather variables (temperature and heat transfer coefficient, obtained from wind speed) were used as inputs in the conceptual thermal resistance model of the setup. The analytical thermal resistance modeling, along with the obtained results during the study, are discussed in Chapter 5.

4.2 Critical Model Assumption

An important assumption in this study is that the proposed hydronic system in DFW area is designed as a preventive measure. This means that the bridge deck will be pre-heated to temperature above freezing during the snowfall and any snow falling on to the bridge deck will immediately melt. Hence, this numerical study excludes any consideration for snow accumulation and latent heat of phase changes. The study only focuses on the heat transfer within the bridge deck, more specifically the spatial distribution of heat and temperature on the bridge deck due to the geothermal hydronic system.

Another assumption in the numerical model is that the interface connections (pipe to concrete at top and pipe to insulating foam at bottom) are perfect. This is reasonable since the PEX pipes have been tightly clipped to the bottom of the concrete slab at close spacings and then encapsulated with thick foam on all sides. Hence, no thermal contact layers have been considered in the numerical model.

4.3 Model Geometry and Material Properties

A numerical 3-dimensional model of geothermal bridge deck that imitates experimental bridge deck was developed as shown in Figure 4.1. The dimension of the concrete bridge deck is 1.8m x 1.2m x 0.1016m. The embedded polyethylene (PEX) pipe, with 1.905 cm outer diameter, 1.27 cm inner diameter and 0.16 m center to center spacing, is embedded in the bridge deck in a meandering pattern. Insulating foam is used as an insulating material at the bottom of the bridge deck to prevent heat dissipation at the bottom. The dimensions of the insulating foam adopted in the model are 1.5m x 1.2m x 0.152m. Circulating water at constant flow rate of 7.5 liters (2 gallons) per minute through the pipe is used as heat source in the model. The main heat transfer mechanism of this model is a three-step procedure discussed below:

i) Initial heat transfer from the circulating water to the pipe by convection

ii) Subsequent heat transfer from the pipe to the concrete slab surface (at top) and pipe to insulating foam (at the bottom) through conduction

iii) Heat transfer from concrete surface (at top) and insulating foam (at bottom) to air by radiation.

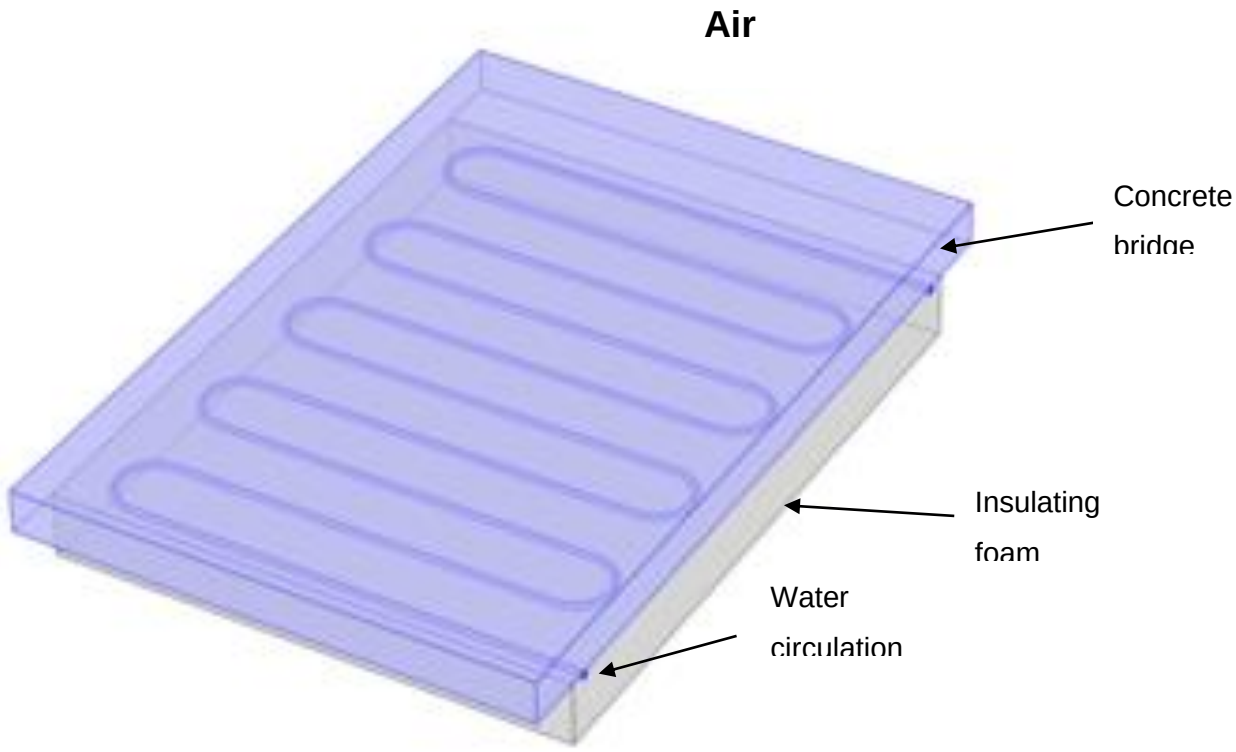

Figure 4.1 Configuration of geothermal heated bridge deck.

The material properties assigned to the model are summarized in Table 4.1. These material properties have been selected based on specification of materials used in the field study by Li., et al., 2018. Since identical materials were used for the present study, same material properties were adopted.

Table 4.1 List of the material properties used in numerical simulations (Li., et al., 2018)

Material	Thermal Property	Value (unit)
Concrete	Density	2300 kg/m^3
	Thermal Conductivity	1.8 W/(m*K)
	Heat Capacity at constant Pressure	880 j/(kg*k)
	Surface Emissivity	0.91
Foam	Density	20 kg/m^3
	Thermal Conductivity	0.03 W/(m*K)
	Heat Capacity at constant Pressure	1300 J/(kg*k)
	Surface Emissivity	0.60
Polyethylene (PEX) Pipe	Density	1350 kg/m^3
	Thermal Conductivity	0.19 W/(m*K)
	Heat Capacity at constant Pressure	950 j/(kg*k)
Water (liquid)	Density	1000 kg/m^3
	Thermal Conductivity	0.6 W/(m*K)
	Heat Capacity at constant Pressure	4185.5 j/(kg*k)
	Ratio of Specific Heats	1.0
	Dynamic Viscosity	0.001 (pa*s)

To simulate experimental conditions, a transient model was simulated in COMSOL using the installed ambient thermocouple data as a boundary condition. Wind speed data was collected from NOAA (National Oceanic and Atmospheric Administration) and Weather Underground data

for DFW Airport, which is located 20 miles from the test site. To compare numerical model outputs, specific points were assigned in the 3D numerical model that mimics the location of the thermocouple in the experimental bridge deck. The initial temperature of the concrete bridge deck, pipe and insulating foam were considered same as the ambient temperature. The flow rate of the water in the inlet was sustained around 7.5 liters (2 gallons) per minute. The initial velocity and water pressure were adjusted zero. Conjugate heat transfer and non-isothermal flow mechanism were adopted to simulate the model. Since fluid is forced to flow over the concrete surface and in the pipe loop, therefore, external and internal forced convection mechanisms were used. Heat transfer coefficient was not assigned to the model as COMSOL calculated the heat transfer coefficient from the fluid velocity input. Perfect contact was assumed between concrete and the PEX pipe interface, and PEX pipe and insulating foam interface. Additional thermal contact between these interfaces were not considered in the simulation.

4.4 Generating Mesh in COMSOL 3D model

Meshing is an important step in any finite element model. The Finite element mesh is applied to subdivide the model into smaller domains called elements. Physical equations are then applied to these elements for iterative solution. Hence, reduction in size of these elements can enhance the accuracy of the solution. Also, compatibility between the adjoining element boundaries reduces complexity of the iterations and reduce computational time. This is termed as refining of mesh. A refined mesh has two distinct benefits – increased accuracy and decreased computation time.

Figure 4.2 illustrates the mesh and the resulting elements in the numerical model for this study. The interface between the outer periphery of pipe surface and adjoining concrete surface is the most important and complex part of this 3D model, as the two heat transfer mechanisms (conduction, convection) work simultaneously at this location. Hence, a free triangular mesh using local size attribute was applied in this interface to reduce element size (Figure 4.3). To further refine the resulting mesh, extra fine predefined swept mesh is applied in the entire pipe loop

domain. To maintain the accuracy of the entire model in line with the pipe loop, extra fine free tetrahedral mesh using local size attribute was used in both concrete deck slab and insulating foam boundary. The finished mesh consisted of 21,944 elements for this model.

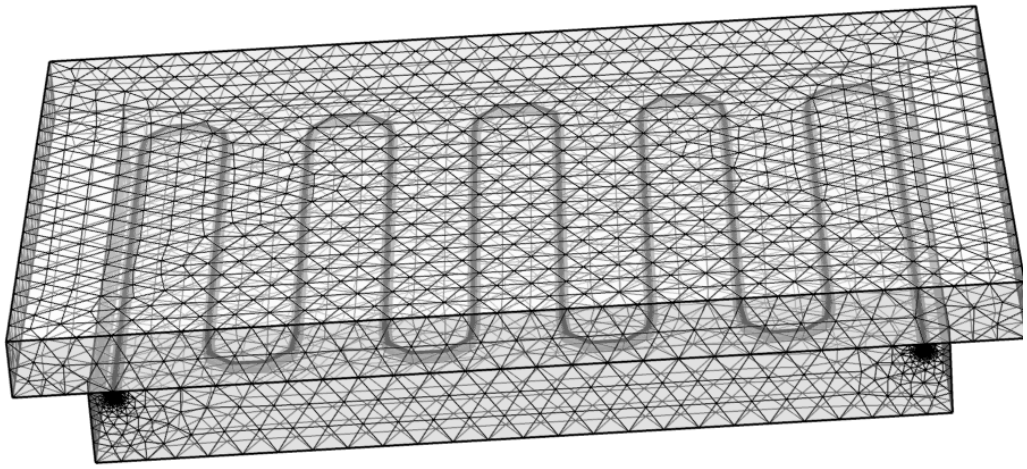

Figure 4.2 Generating meshing in bridge deck

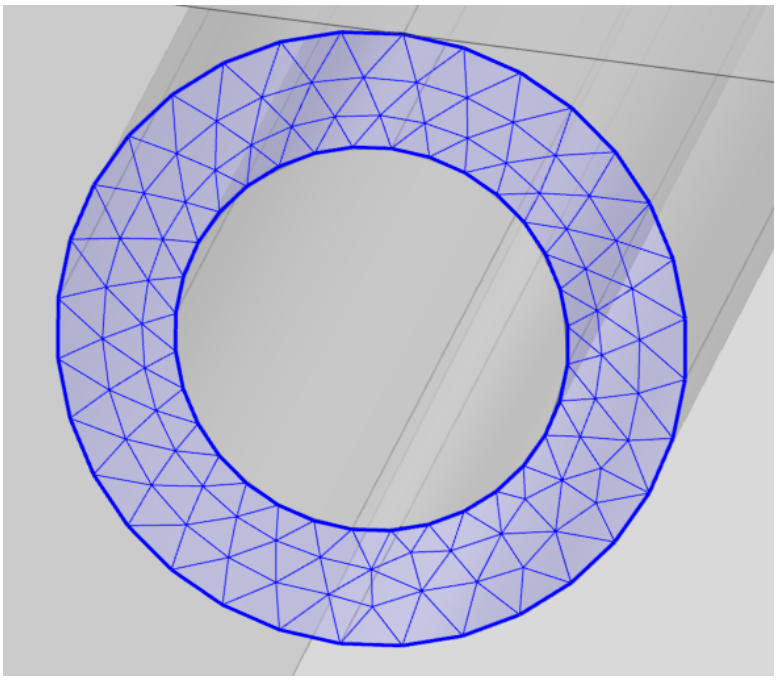

Figure 4.3 Zoomed view of inlet mesh

The recorded ambient temperature and wind speed for all three weather events (Pre-Test,

Winter simulation and Cold Front) were used as inputs in this transient numerical model. After the successful convergence of the model simulation, the temperature output from the pre-determined locations was obtained and compared against the installed thermocouple outputs in the experimental bridge deck for model verification. After the numerical model was verified to produce reasonably consistent results compared to the experimental bridge deck, historical weather data of coldest days of the last 5 years were simulated in the model. The outputs were analyzed to assess the efficiency of the system to extreme weather events from 2014-2018.

The results obtained from the numerical model and their interpretations are discussed in detail in Chapter 5.

Chapter 5.
Results and Discussion

5.1 Introduction

This chapter discusses the results obtained from the experimental deck slab, the numerical model simulation from COMSOL Multiphysics and the analytical resistance model. First, the results obtained from the experimental deck slab are compared to the numerical model results from COMSOL and the numerical model is validated by the three weather events (Pre-test, Cold front and Winter Simulation). This validated model is then utilized to predict the performance of the proposed de-icing system against the most extreme weather events in the last five years. Finally, an analytical model is presented for the de-icing system setup and all three results (experimental, numerical and analytical) are compared for a complete understanding of the setup and its behavior.

5.2 Validation of Experimental result with Analytical Model using thermal Resistance

After successful verification of the numerical model developed in COMSOL, an attempt was made to develop an analytical model to estimate the surface temperature of the deck slab and compare the output of the proposed analytical model with the obtained experimental results. As described earlier in the Chapter 3, the thermal resistance of cylindrical coordinate system was utilized to evaluate the surface temperature of the bridge deck. Figure 5.0.1 illustrates the basic principle of this modeling technique, where the thermal properties of each layer is modeled as an equivalent electrical resistance.

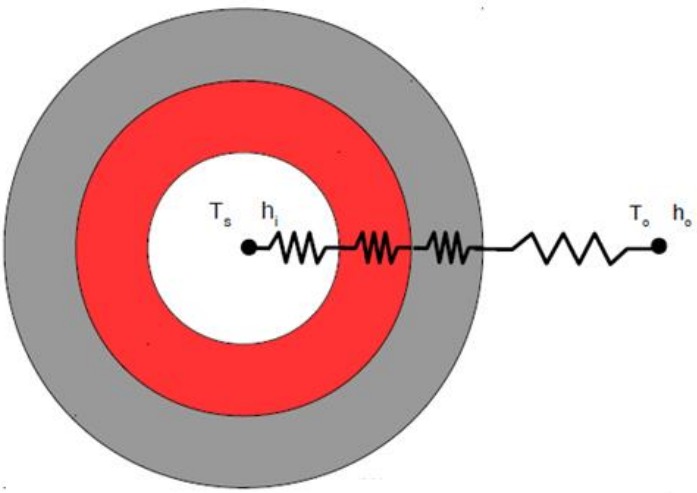

Figure 5.0.1 Illustration of principle of thermal resistance modeling

Figure 5.0.2 shows the actual thermal resistance model for an embedded hydronic system.

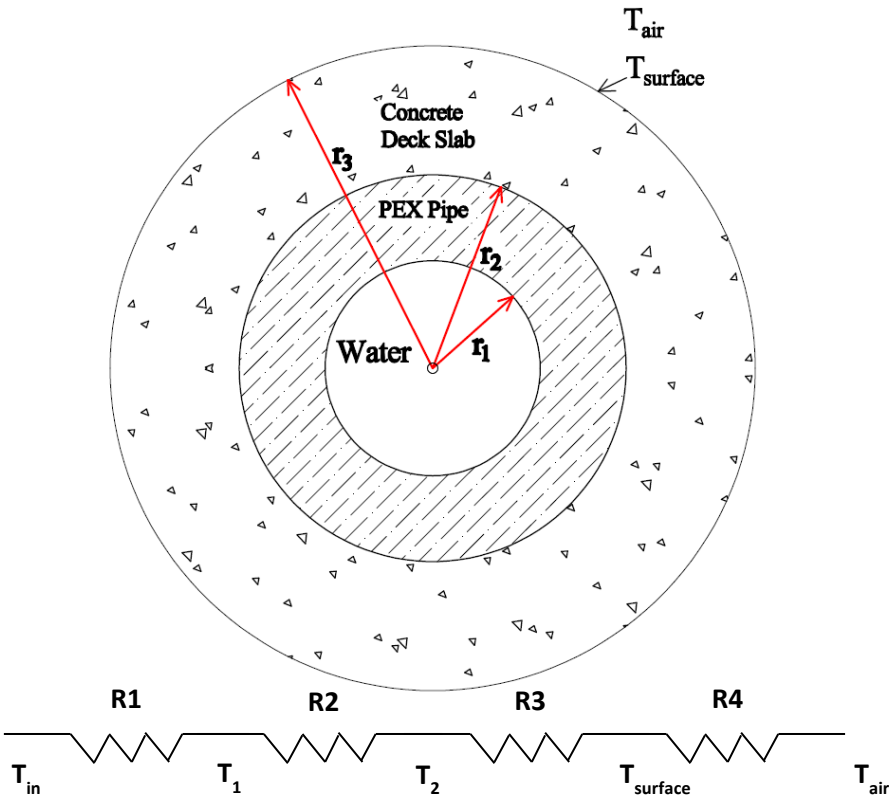

Figure 5.0.2 Analytical thermal resistance model for embedded hydronic heating system

The dimension of the above model and material properties are described in Table 5.1

Table 5.1 Input model parameters for Analytical Model

Model Parameter	**Value**
Radius of the inner pipe	0.00635 m
Radius of the outer pipe	0.009525 m
Radius of concrete deck slab (concrete deck slab was considered circular to keep uniformity of the radial system.	0.1111 m
Thermal conductivity of concrete	1.8 w/(m.k)
Thermal conductivity of PEX pipe	0.19 w/(m.k)
Heat transfer coefficient of water	3000 w/(m^2.k)
Heat transfer coefficient of air (Average of the range of results obtained from COMSOL during entire simulation)	31 w/(m^2.k)
Velocity of water	0.9962 m/s
Inlet temperature	32°C
Ambient Temperature	Experimental data used from Cold front event

The heat transfer rate equation for multilayer radial system can be expressed as

$$q = \frac{T_{inlet} - T_{Air}}{R1+R2+R3+R4} \qquad \text{(Equation 50)}$$

$$q = \frac{T_{inlet} - T_{Air}}{\frac{1}{2r_1\pi h_i} + \frac{\ln(\frac{r_2}{r_1})}{2\pi k_A} + \frac{\ln(\frac{r_3}{r_2})}{2\pi k_B} + \frac{1}{2r_3\pi h_o}} \qquad \text{(Equation 51)}$$

Here,

R_1= Convection Resistance through Inner diameter of the Pipe = 0.00696 K/Watt

R_2 = Conduction Resistance between inner and outer diameter of the pipe = 0.28303 K/Watt

R_3 = Conduction Resistance between outer diameter of the pipe and concrete slab = 0.15680 K/Watt

R_4 = Convective Resistance between Concrete Slab and Air = 0.02368 K/Watt

The surface temperature of the concrete slab can be described by Equation 52

$$q=\frac{(T_{surface} - T_{Air})}{R_4} \qquad \text{(Equation 52)}$$

However, since our proposed system will be attached to the base of the slab, there will be no concrete on the bottom half of the pipe. Hence, the model needs to be modified to fit our purpose. Since the proposed external system is attached to the bottom of the slab, the contact surface between the pipe and the deck slab is essentially a narrow rectangle. Hence, to prepare an analytical model, an estimation of proper contact area between the pipe and the slab surface is necessary.

In order to accurately estimate the contact surface between the pipe and the slab, a scaled model of the pipe and the slab were first drafted in AutoCAD. The contact area of the pipe with the slab was then determined. The central angle of the contact area, in shape of a pie, was then determined from AutoCAD (Figure 5.0.3)

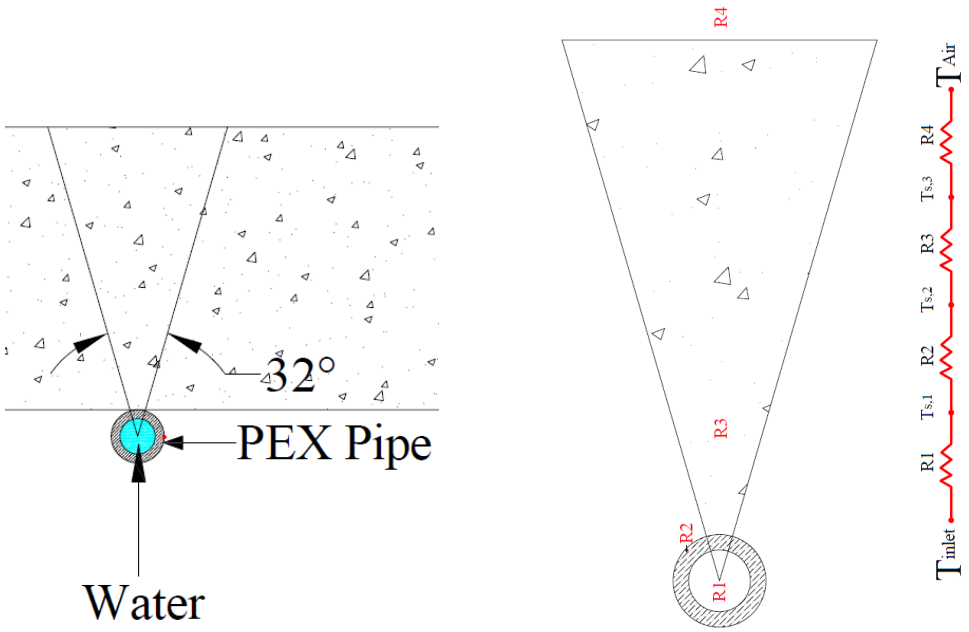

Figure 5.0.3 Analytical thermal resistance model for externally attached hydronic heating system

Based on Figure 5.0.3, the heat transfer rate equation also needs to be modified for our purpose, as the effective perimeter for heat transfer has been reduced to a fraction of the full circle. Since the extended central angle of the contact area is 32º, the ratio of the circumference of the contact zone to the full circle is 0.088. The new equation becomes

$$q = \frac{T_{inlet}-T_{Air}}{\frac{1}{0.088\times 2r_1\pi h_{water}}+\frac{\ln(\frac{r_2}{r_1})}{0.088\times 2\pi k_{pipe}}+\frac{\ln(\frac{r_3}{r_2})}{0.088\times 2\pi k_{concrete}}+\frac{1}{0.088\times 2r_3\pi h_{air}}} \quad \text{(Equation 53)}$$

From Equation 53, the heat transfer rate of the system can be determined. Now, from the principle of conservation of energy, we can conclude that heat will be transferred perfectly between the material boundaries, and hence, each component of heat transfer will be equal to the others. Equation 54 then holds true.

$$q=\frac{T_{inlet}-T_{s1}}{\frac{1}{0.088\times 2r_1\pi h_{water}}}=\frac{T_{s1}-T_{s2}}{\frac{\ln(r_2/r_1)}{0.088\times 2\pi k_{pipe}}}=\frac{T_{s2}-T_{s3}}{\frac{\ln(r_3/r_2)}{0.088\times 2\pi k_{concrete}}}=\frac{T_{s3}-T_{air}}{\frac{1}{0.088\times 2r_1\pi h_{air}}} \quad \text{(Equation 54)}$$

Therefore,

$$q=\frac{T_{s3}-T_{air}}{\frac{1}{0.088\times 2r_1\pi h_{air}}} \quad \text{(Equation 55)}$$

$$T_{s3}=T_{air}+(q\times 0.088\times 2\times r_3\times \pi\times h_{air}) \quad \text{(Equation 56)}$$

Figure 5.0.4 compares the experimental results obtained from the deck slab with the analytical model results obtained using each data point as an individual input into Equation 56.

As we observed from the Figure 5.0.4, the analytical result closely matched with experimental results due to the modified geometry of the model mimicking actual setup.

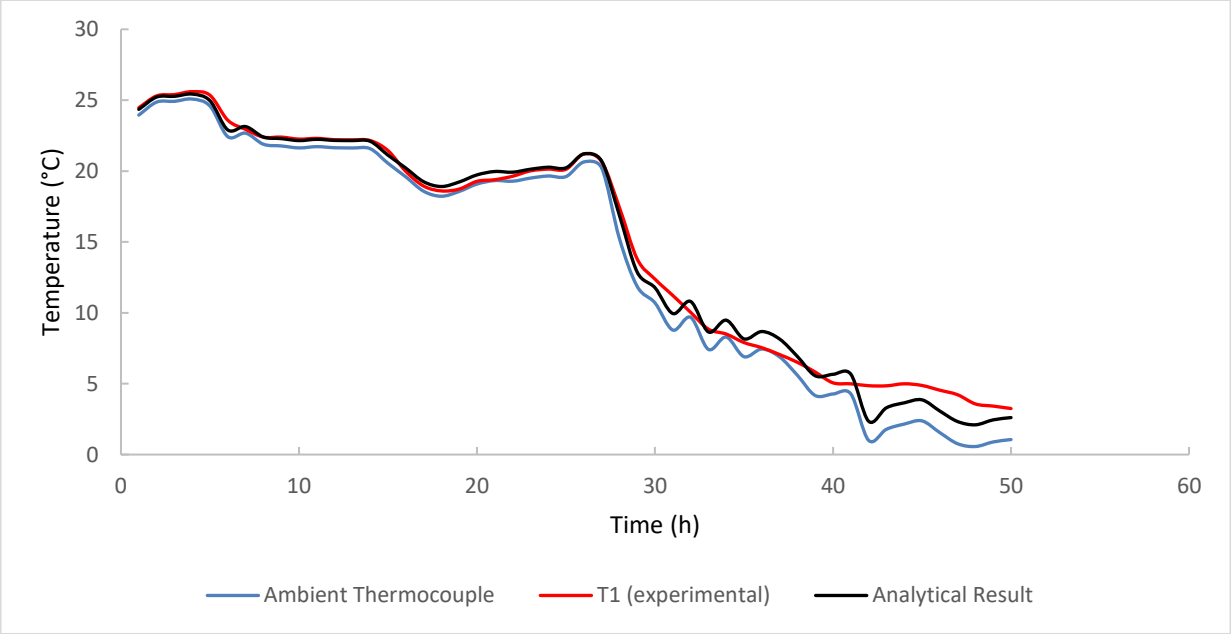

Figure 5.0.4 Comparison between Experimental Result and Analytical Result

5.3 Validation of the numerical model in different weather condition

5.3.1 Pretest Event

The pretest was performed to observe the fluctuation of concrete slab temperature to transient ambient temperature. In this event, the concrete slab, without any insulating foam at the bottom or heated water circulation, was placed outdoors. The thermocouple temperatures were continuously recorded. Ambient temperature and wind speed obtained from the ambient thermocouple and weather database respectively were used as model inputs in the COMSOL Model. The event was recorded for three days to capture the diurnal cycles and its effect on the concrete slab. Figure 5.0.5 shows the experimental setup for the pre-test, without any insulating foam at the bottom or any external water circulation. Figure 5.0.6 plots the experimental and COMSOL results obtained from the pre-test event at 0.5” depth from the surface at thermocouple location T1. Other locations follow the same trend, and hence have not been shown for clarity of Figure 5.0.6.

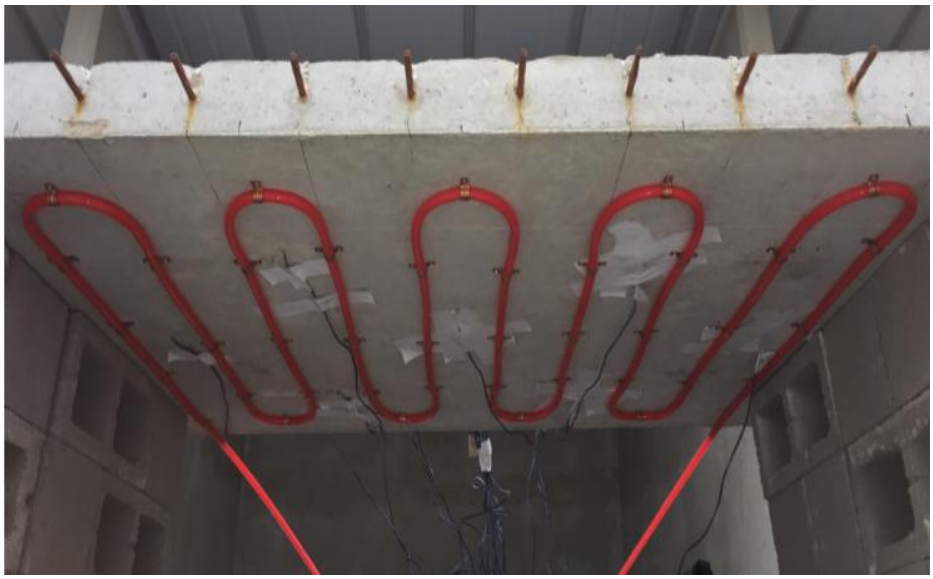

Figure 5.0.5 Pre-Test Experimental Setup

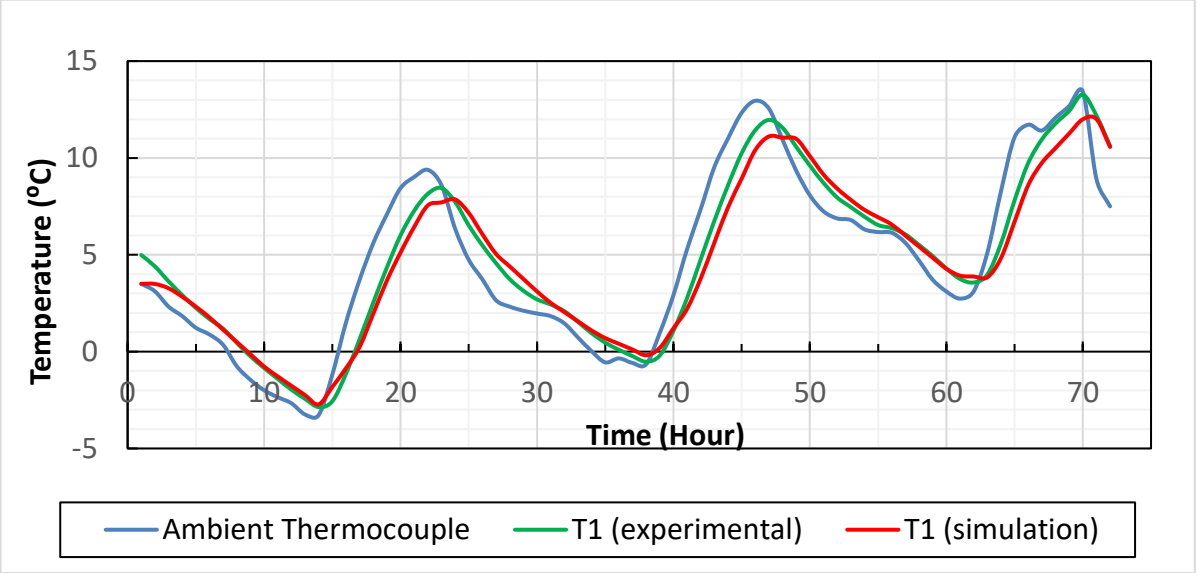

Figure 5.0.6 Variation of slab temperature during Pre-test event (0.5" depth from slab surface)

From the plot, it is evident that the numerical simulation results followed the cyclic trend of the ambient thermocouple pattern. It also matched closely with the experimental results. However, there is a well-defined time lag between the ambient temperature and both experimental and numerical simulation. The reasoning for the time lag is lower thermal conductivity of concrete (1.8 w/m.k). Due to lower thermal conductivity, the concrete deck slab took a certain amount of time to absorb heat from the environment. Similarly, it took time for dissipation of heat when the ambient temperature decreased. Consequently, the slab temperature was greater than environmental temperature during the night cycle and lower than environmental temperature in the morning cycle. Figure 5.0.6 clearly follows the expected trend.

5.3.2 Cold Front Event

After the pre-test, close cell foam was used to seal the PEX pipes at the bottom to simulate application of insulating foam. There was a cold front which occurred from 19th February 2018 to 21st February 2018. At the time of cold front, the temperature dropped from 22°C to 9°C within a 20-hour interval on the night of February 20th. The water tank was set to 32°C to observe the

overall performance of the bridge deck at the time of cold front. The efficiency of the de-icing in geothermal bridge deck is inversely proportional to the change in temperature gradient. The greater change in temperature gradient within the slab, the lower the efficiency and vice versa. Figure 5.0.7 to Figure 5.0.10 show the temperature change in bridge deck at different hour interval.

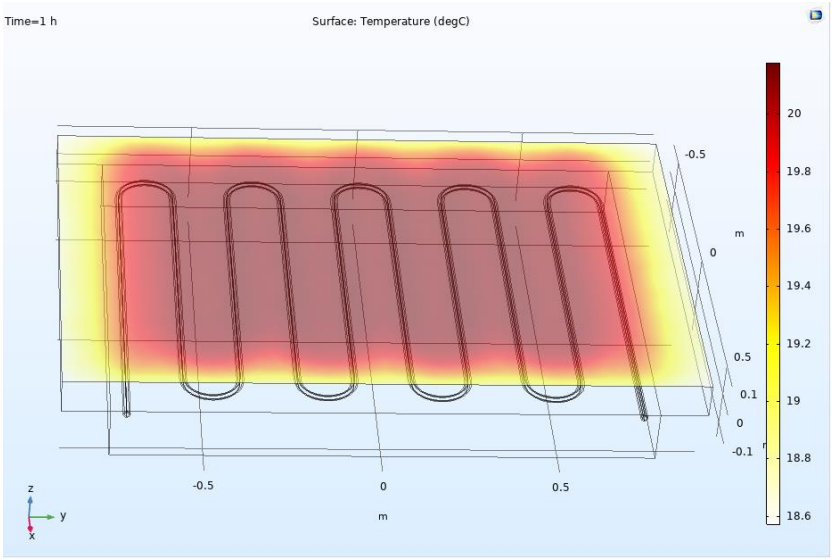

Figure 5.0.7 Temperature Change in bridge deck after 8 hours

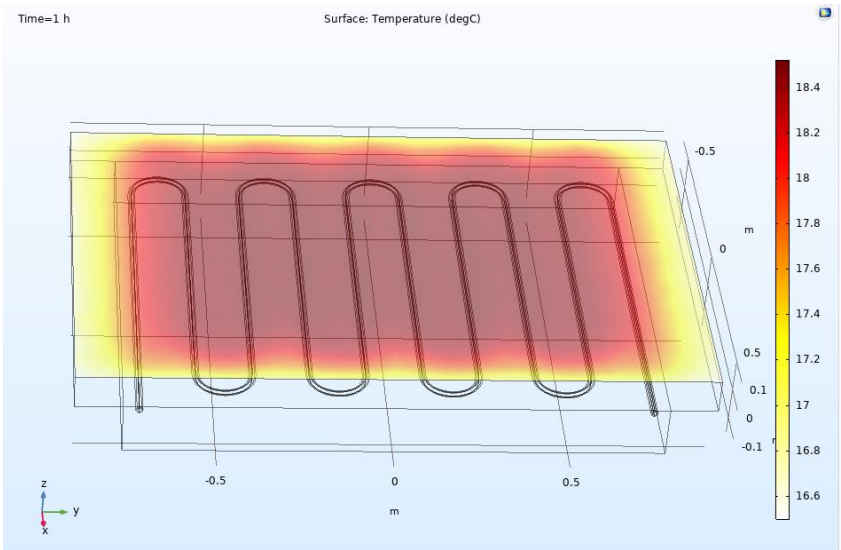

Figure 5.0.8 Temperature Change in bridge deck after 16 hours

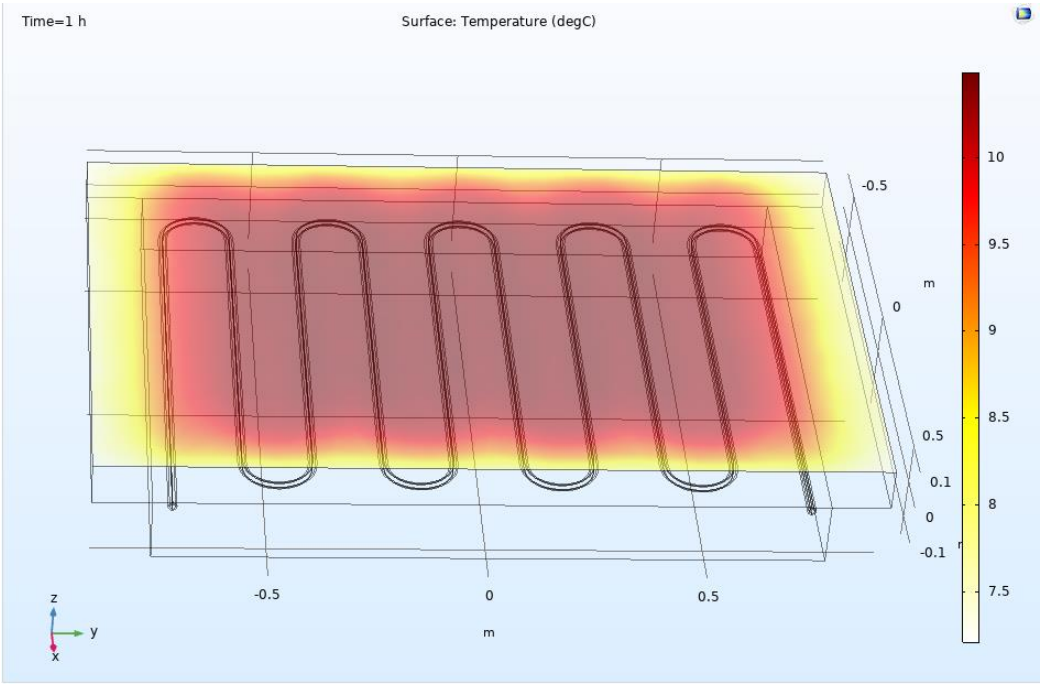

Figure 5.0.9 Temperature Change in bridge deck after 24 hours

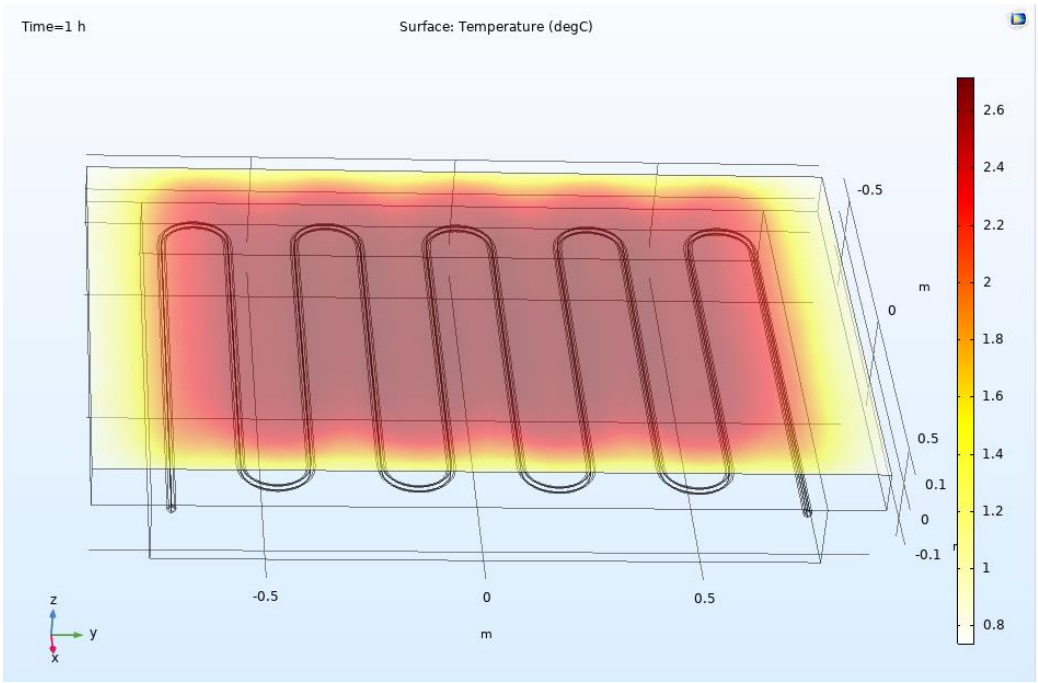

Figure 5.0.10 Temperature Change in bridge deck after 38 hours

The main objective of the setup was to maintain the bridge deck temperature above freezing boundary. To observe the slab temperature, seven thermocouples were installed at 0.5-inch depth from the top of the slab surface. Figure 5.0.11 shows that the numerical results and experimental results on the thermocouple location T1. Since other thermocouples follow similar trend, they were not included in the figure for clarity.

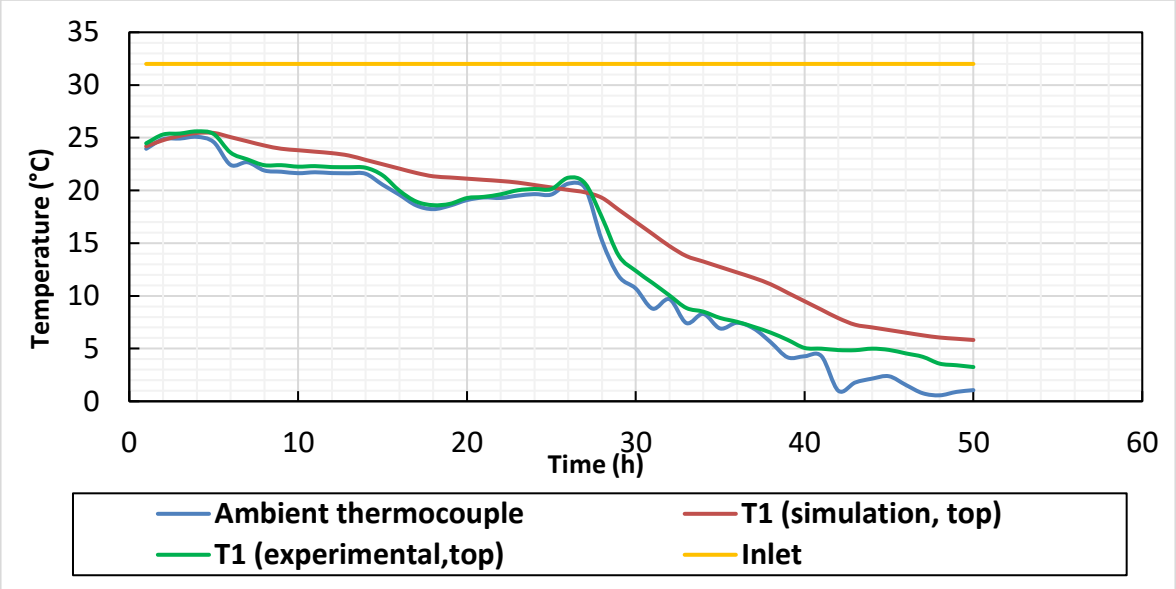

Figure 5.0.11 Comparison between Experimental result and Numerical result with respect to ambient temperature at thermocouple 1

From figure 5.0.11, it is observed that all three independent variables (ambient temperature, experimental testing and simulation results) follow similar trend. The maximum variation between experimental and numerical test results between all four thermocouples was 5ºC. However, there were zones where both simulation and testing results exhibited a diverging trend with the ambient thermocouple for all four locations.

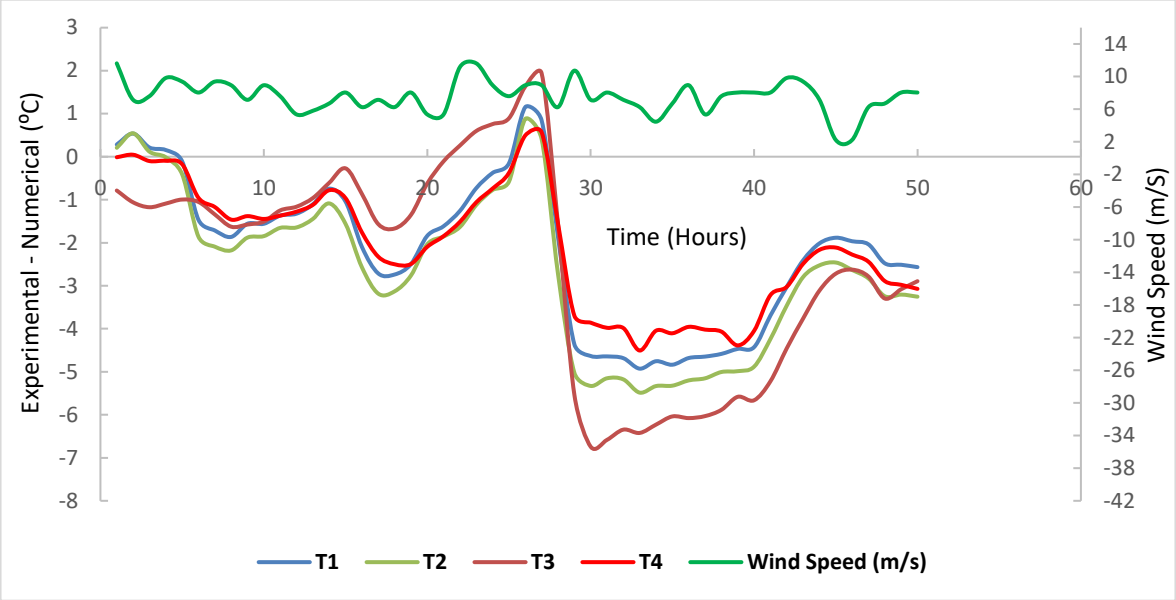

Figure 5.0.12 Deviation of Numerical results from Experimental Results for Thermocouples

It is evident from Figure 5.0.12 that all thermocouple locations exhibited the same deviations at identical times. Consistent diverging trend observed between 15-20 hours and 28-40 hours. Moreover, maximum variation between experimental results and numerical simulation occurred at 30th hour for all thermocouples. Also, the variations between experimental and numerical simulations occur when there is steep drop of temperature, indicating higher convective loss in the experimental setup for all thermocouples. This verifies that the reason for divergence is identical for all thermocouples.

There are two principle points of variation between the experimental results and numerical simulation. Firstly, the wind speed data for the numerical simulation was obtained from the weather database located at DFW airport, which is about 20 miles away from the test site. Local wind variations affected the experimental results, which was not the case for numerical simulation inputs. Secondly, thermocouple data readings were continuous, whereas numerical inputs were discrete between time steps. Due to these two reasons, there are differences between the thermocouple readings and corresponding numerical simulation results, although they seem to be within reasonable agreement.

Since the experimental setup allows us to see temperature distribution within the slab, experimental and numerical simulation results of top and bottom thermocouple for thermocouple locations T1 is plotted in Figure 5.0.13.

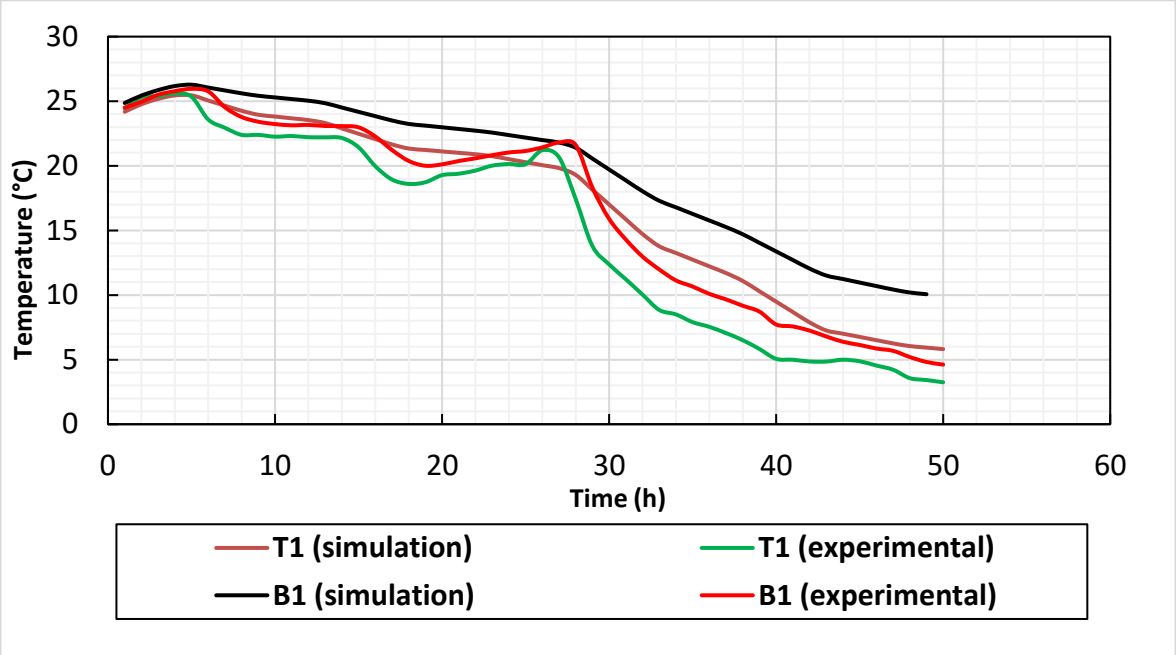

Figure 5.0.13 Vertical Temperature distribution for Thermocouple T1

From Figure 5.0.13, it is observed the top and bottom thermocouples show the expected trend (higher temperature at the bottom thermocouple than top thermocouple). Confirmation of this trend verifies proper heat distribution in the slab in the numerical model.

5.3.4 Winter Simulation

The winter event occurred on February 11-12, 2018. Due to a cold front that elapsed few nights before the winter event, the ambient temperature was below 0 degree Celsius each night. While a snow gun was applied to create cold mist at the top of the slab to simulate winter event experimentally, the mist was not simulated in the COMSOL to simplify the model. It was assumed that any snow that falls on the slab will melt instantaneously due to the elevated temperature of

the slab.

In order to simulate the pre-heating of the slab, the average ambient temperature and wind speeds 18 hours prior to the start of the event was determined from the weather database. The model was run for 18 hours with the constant weather inputs (average temperature and average wind speeds of the past 18 hours) to simulate the pre-heating of the slab. From this 18-hour simulation, the initial slab temperature was determined for the winter simulation model run.

With the obtained initial temperature of the slab, the transient weather inputs, ambient thermocouple temperature data and wind speed data obtained from weather database, were applied to the model. However, there was excessive fluctuation of the ambient temperature due to sprayed mist, which was not modeled in the simulation (Figure 5.0.14). Hence, to counteract the effect of the temperature fluctuation due to the mist, an average constant temperature of -1.76ºC was used from hour 5 onwards. Also, constant heat transfer coefficient was assumed to counteract the effect of local wind variations. The results of the simulation are presented in Figure 5.0.14.

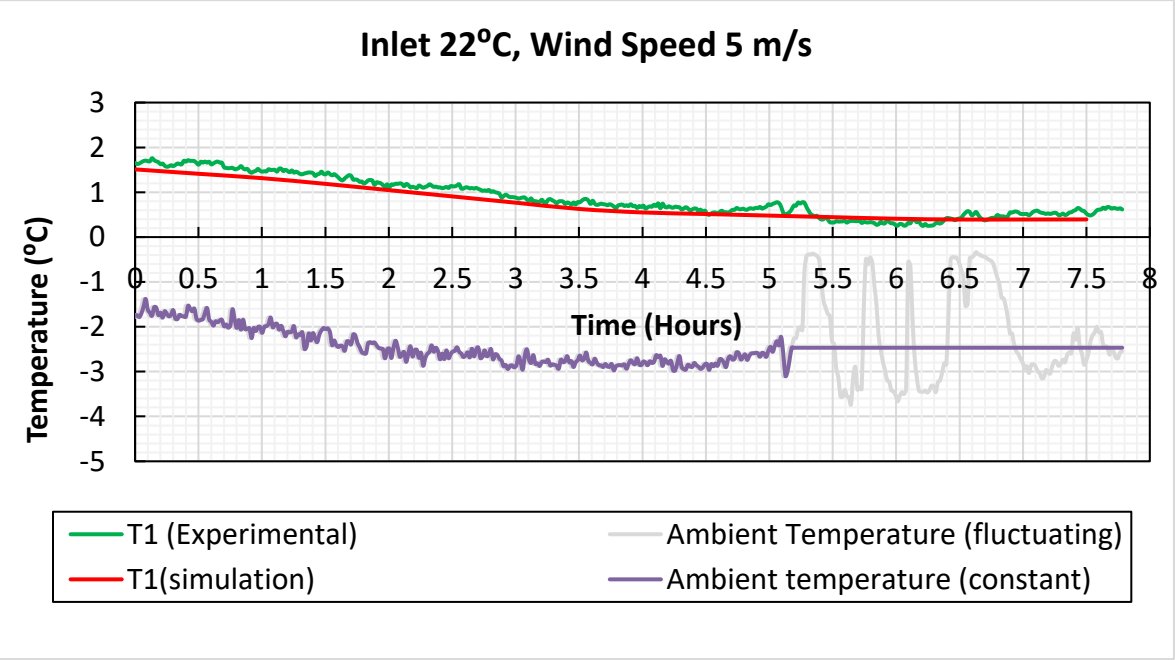

Figure 5.0.14 Temperature variation of thermocouple T1 during winter simulation event

As we saw in the earlier experimental design (Figure 3.8), the ambient temperature was in stabilized condition before the application of snow event and all thermocouple followed the similar trend. Inlet temperature was maintained around 22°C during the event.

From Figure 5.0.14, it can be observed that the experimental and simulation results matched closely for the entire winter event. This was possible due to constant temperature assumption during the snow gun spray period. Since the model did not account for the mist, it was able to accurately predict the slab temperature with the provided inputs.

5.4 Analysis of insulation effect

The insulating material plays a very important role in de-icing geothermal bridge deck problem. It prevents the dissipation of heat underneath the bridge deck. It was desirable to understand the contribution of the insulating foam at the bottom to the efficiency of the hydronic system. Since an accompanying experimental study was not available, the verified numerical model was run with two different scenarios: a simulation with the insulating foam at the bottom and another without any insulating foam at the bottom. From analysis of result differences between these two model runs, a preliminary idea can be obtained about the role of insulating foam in the system. Identical pre-test inputs (ambient temperature and wind speed) were used for the study. The results of the COMSOL model simulations (Thermocouple location T1 at 0.5” depth from the top of the slab) are presented in Figure 5.0.15.

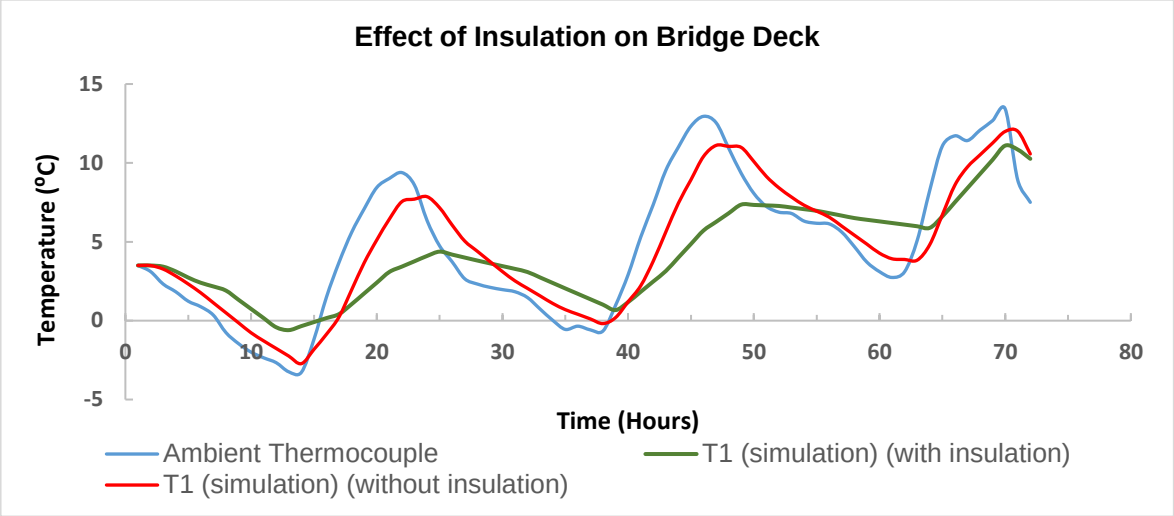

Figure 5.0.15 Contribution of the insulating foam insulation to the efficiency of the proposed system

As we observed from the Figure 5.0.15, the numerical results without insulation closely follow the ambient temperature, with a minimal time lag. However, the numerical results with insulation (insulating foam) show a pronounced time lag, both with ambient temperature and simulation without insulation. Also, the slope of the temperature gradient is lower in slab temperature with insulating foam than the slab temperature gradient without insulating foam. Moreover, the minimum slab temperature with insulating foam was observed at a time slightly later than the minimum slab temperature without using insulation in response to the ambient temperature. All three above discussed trends indicate that use of insulating foam obstructs heat changes and tries to maintain constant temperature in the slab system.

5.5 Prediction of de-icing efficiency of the proposed system in the historical extreme weather events in DFW area

This section predicts de-icing efficiency of the proposed system in the extreme weather events from the historical data of extreme weather events from 2014 to 2018. To account for the extreme weather conditions in DFW area for the last 5 years, the air temperature and wind speed were collected from NOAA (National Oceanic and Atmospheric Administration) and Weather

Underground database for DFW Airport. To maintain the transient nature of the data, simulation data input was initiated from a day before the coldest day of each year and was continued up to 2 days after the event completion. To anticipate the de-icing performance of the geothermal bridge deck, the system was assumed to be in operation 24 hours before the starting of the extreme weather event. Figure 5.0.16 to 5.0.22 depicts the prediction of de-icing efficiency of the proposed geothermal bridge deck for the last 5 years.

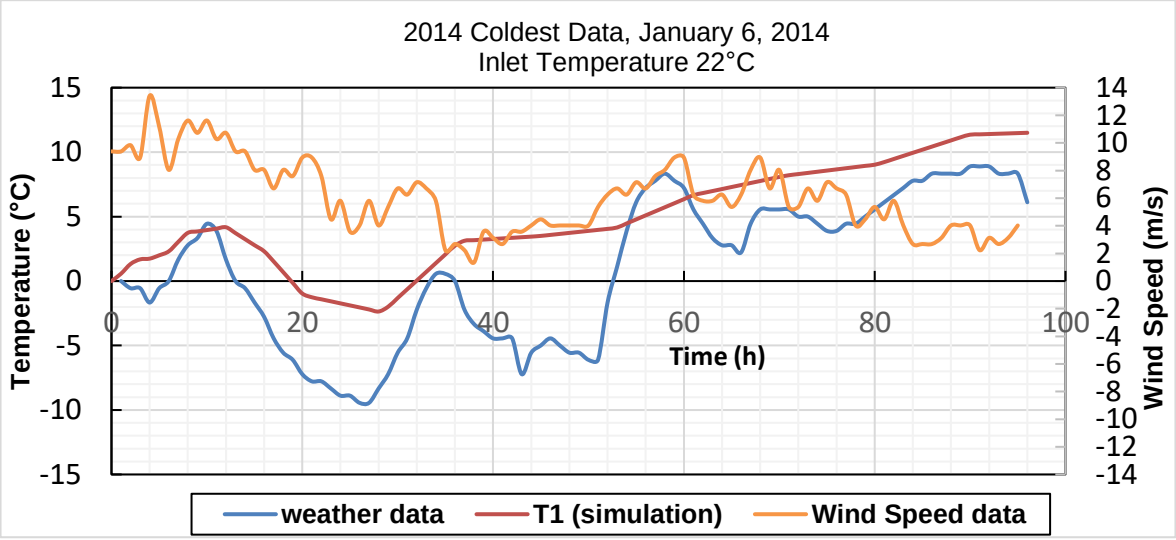

Figure 5.0.16 Weather data and simulation result from January 5th to January 8th, 2014 (inlet temperature = 22ºC)

January 6, 2014 was the coldest day in 2014. Based on the observation of above Figure 5.0.16, it can be concluded that from 19 to 31 hours into the simulation, the slab temperature was below 0°C. The inlet temperature was considered 22° C, which was not enough for the slab temperature to reach above freezing temperature. After a few iterations, it is observed that to achieve the slab temperature above freezing temperature during the coldest day of 2014, the required inlet temperature is approximately 32°C. The results of the same simulation with 32°C is shown in Figure 5.0.17.

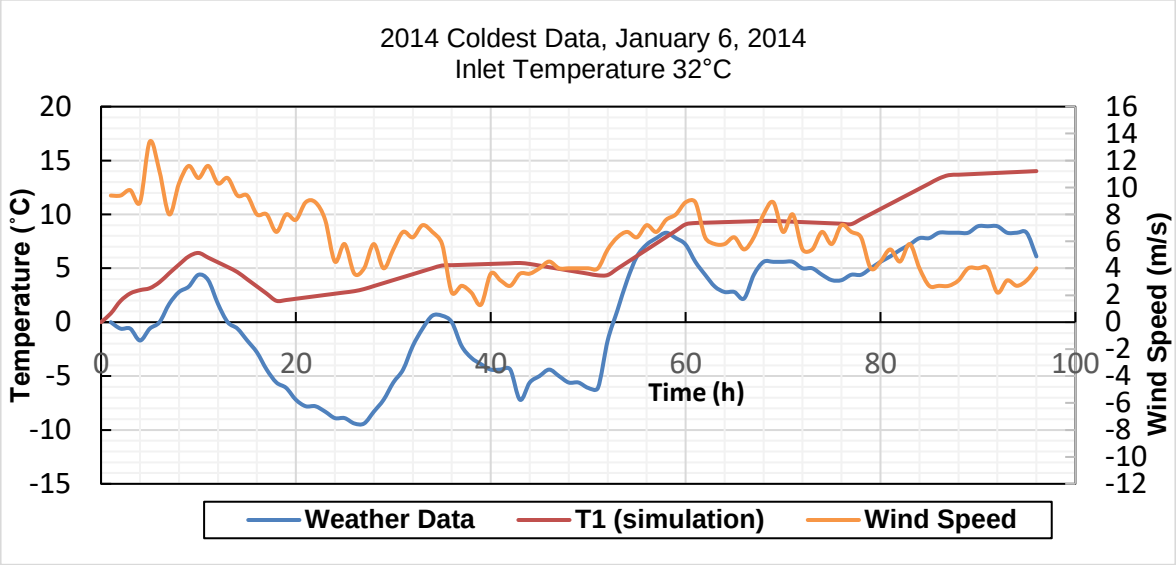

Figure 5.0.17 Weather data and Simulation result from January 5th to January 8th, 2014 (inlet temperature = 32ºC)

Similarly, in 2015, the coldest day was 8th January. As observed from Figure 5.0.18, with 22°C water the bridge deck was over freezing temperature during the coldest day. From Figure 5.0.19 to Figure 5.0.22, it can be concluded that while 22°C water is an acceptable circulation medium to gain the de-icing efficiency of the proposed bridge deck during the coldest days in 2017 and 2018, but with same inlet temperature, the bridge deck risked icing for more than 10 hours in 2014, 2015 and 2016. After some additional iterations, it is found that an inlet temperature of approximately 38°C is required to achieve above freezing temperature in the deck slab in 2016. Table 5.2 summarizes the findings of the predictive simulations for coldest days of 2014-2018.

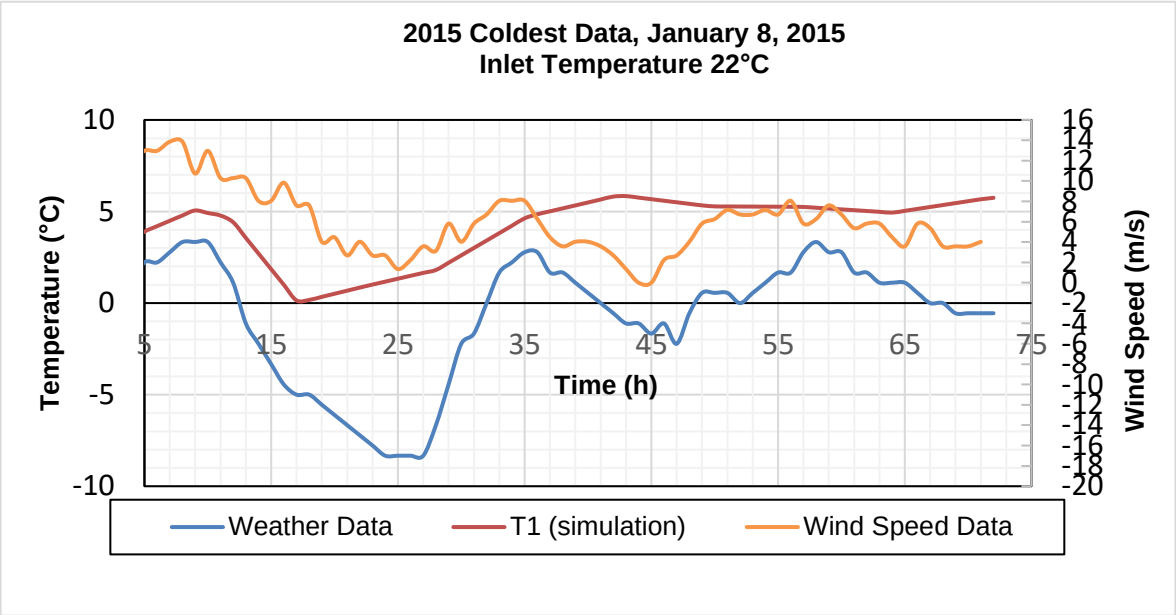

Figure 5.0.18 Weather data and simulation result from January 7th to January 9th, 2015 (inlet temperature of 22°C)

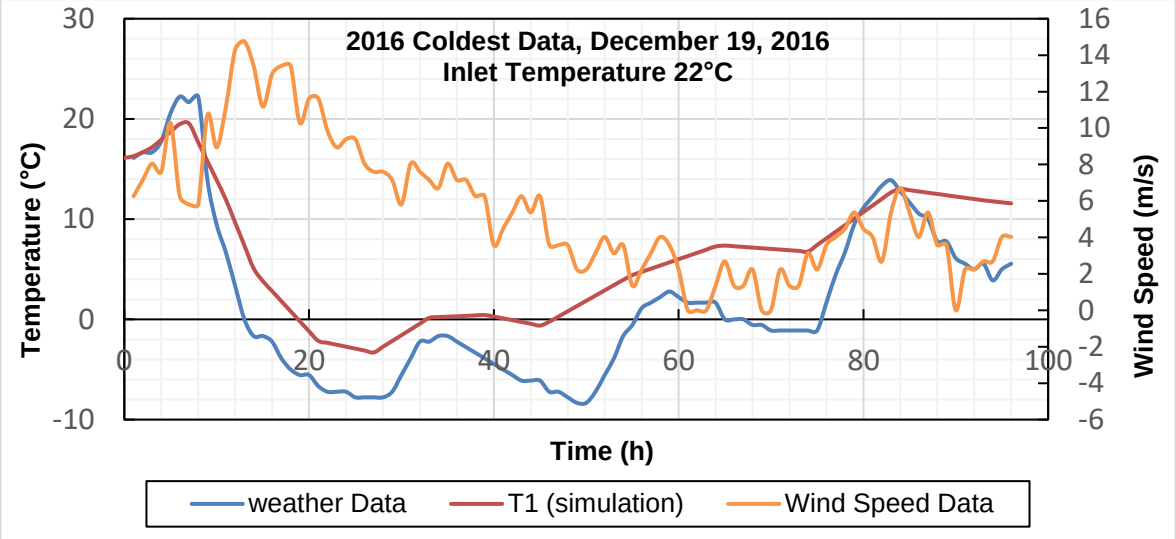

Figure 5.0.19 Weather data and simulation result from December 17th to December 20st, 2016 (Inlet temperature of 22°C)

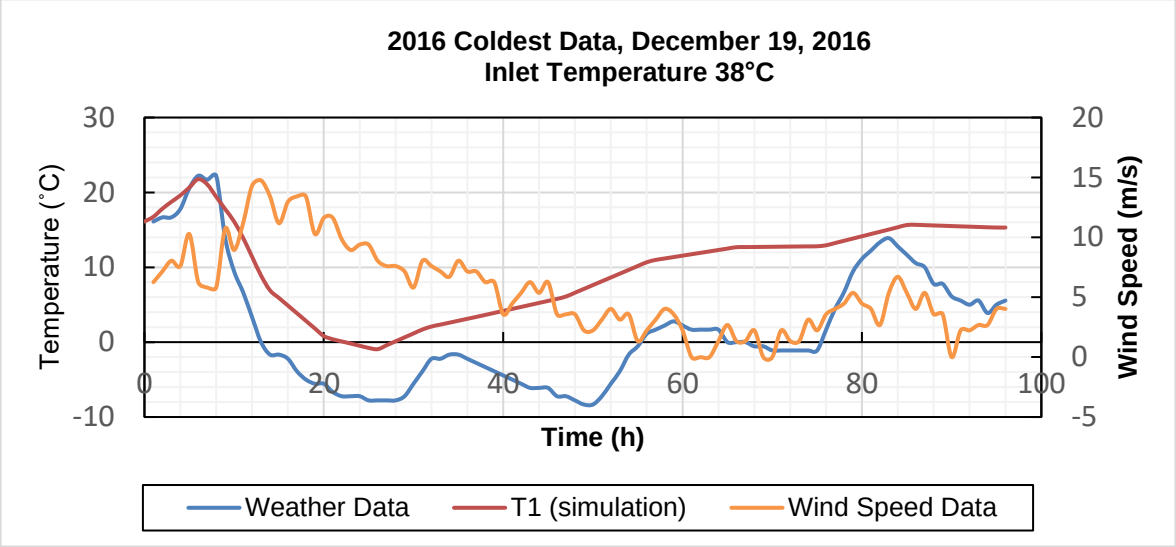

Figure 5.0.20 Weather data and simulation result from December 17th to December 20st, 2016 (Inlet temperature of 38°C)

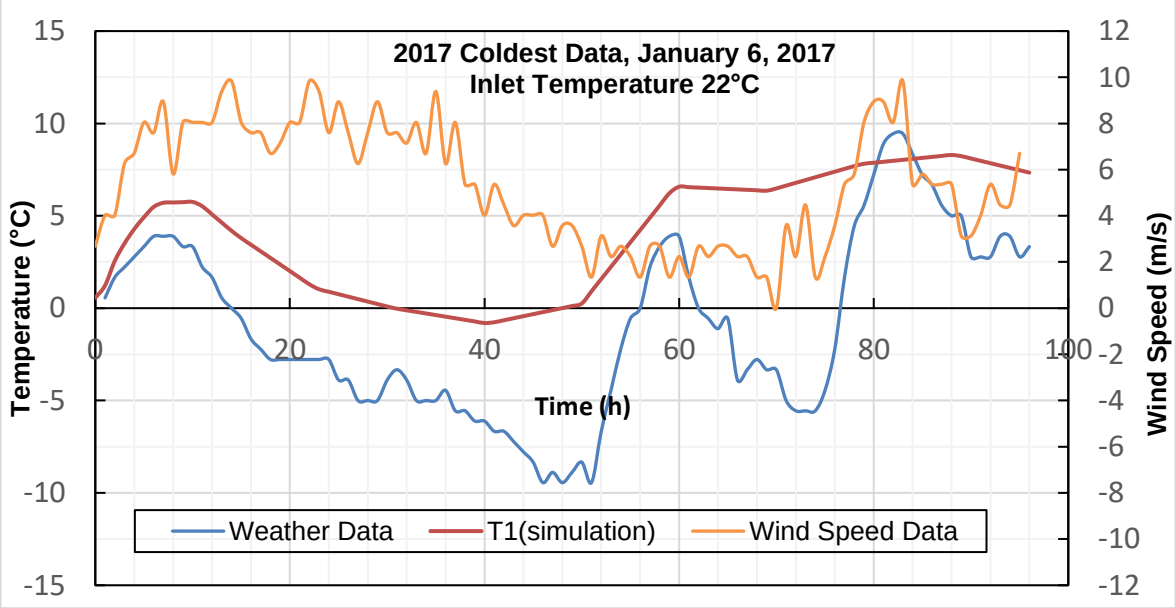

Figure 5.0.21 Weather data and simulation result from January 5th to January 8th, 2017 (Inlet temperature of 22°C)

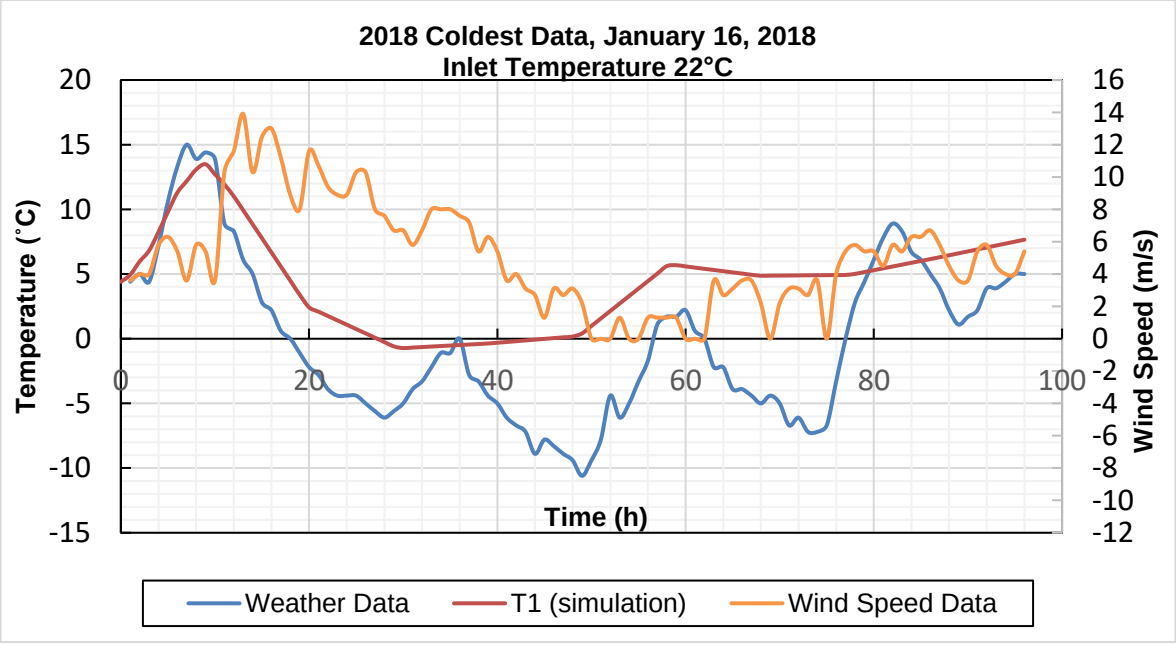

Figure 5.0.22 Weather data and simulation result from January 15th to January 18th, 2018 (Inlet temperature of 22°C)

Table 5.2 Summary of Predictive Winter Simulation for coldest days of 2014-2018

Year	Inlet temperature (ºC)	Lowest Ambient Temperature (ºC)	Minimum Therm. temperature (ºC)	Duration thermocouple below freezing (hours)
2014	22	-9.4	-2.36	13
2014	32	-9.4	0.81	0
2015	22	-8.3	0.14	0
2016	22	-8.3	-3.3	13
2016	38	-8.3	-0.94	4
2017	22	-9.4	-0.80	19
2018	22	-10.6	-0.72	19

Chapter 6.
Conclusions and Recommendations

Summary of Conclusions

The main objective of this study is to develop a numerical model to assess the performance of implementing hydronic heating system for de-icing of bridges in DFW area. To accomplish the objective, an experimental concrete slab was first set up with the proposed hydronic system fitted underneath the slab. A network of thermocouples was then installed at various locations and depths in the slab to obtain temperature distribution in the slab due to the system. The slab was then fitted with a closed cell spray foam to simulate a layer of insulating foam at the bottom. The efficiency of the system was then determined by measuring temperature by the installed thermocouples due to actual weather events. A numerical model was also created in COMSOL to simulate the behavior of the slab. The numerical model was first validated by comparing the temperature results with the experimental slab with identical weather inputs. The validated model was then used to determine the contribution of insulating foam application to the system performance and predict the performance of the proposed system to historical extreme local weather events. An analytical thermal resistance model was also developed for the setup during this study. The results obtained in this study are summarized below:

i) Without any external heat input and insulating foam, the temperature of the concrete slab follows the same trend as the ambient temperature, but with a small time lag due to lower thermal conductivity of concrete.

ii) If insulating foam is present, the time lag is significantly increased, and the system responds slowly to external temperature variations.

iii) The numerical model results agree closely to the experimental results obtained. The average variation between corresponding experimental and numerical results varied between 2ºC and 3ºC for thermocouple locations.

iv) Both the experimental program and numerical analysis confirms that the system is efficient to keep the surface temperature above freezing even during a short

precipitation event.

v) The proposed analytical thermal resistance model also agrees very well with the experimental results.

vi) Prediction from the numerical model with the extreme weather data for the last 5 years shows that a circulation temperature of 22ºC is not always enough to keep the bridge deck temperature above freezing. The required circulation temperature to keep the bridge deck above freezing is about 38ºC for the last five years.

Recommendations for future study

Based on the limitations of the study, the following recommendations are proposed for future study

i) A detailed study may be performed on the sensitivity analysis of the material and thermal properties required during the design of the de-icing system (thermal conductivity of concrete, heat transfer coefficient of air and water etc.).

ii) An experimental study may be performed on the effect of design parameters on the efficiency of the proposed system (pipe spacing, insulating foam thickness, inlet temperature etc.).

iii) Effect of steel reinforcement on the overall thermal performance of the bridge deck can be investigated.

iv) Effect of different circulation liquids (water mixed with differing percentage of glycols and other de-icing liquids) on the system efficiency can also be investigated.

REFERENCES

ASHRAE, A. (1999). ASHRAE Handbook-HVAC Applications. American society of Heating, Refrigerating and Air-Conditioning Engineers.

Bani-Hani, E. H., & Assad, M. E. H (2018). Boundary-Layer Theory of Fluid Flow past a Flat-Plate: Numerical Solution using MATLAB. International Journal of Computer Applications, 975, 8887.

Bergman, T. L., Incropera, F. P., DeWitt, D. P., & Lavine, A. S. (2011). Fundamentals of heat and mass transfer. John Wiley & Sons.

Bowers, Jr, G. A., & Olgun, C. G. (2014). Ground-source bridge deck deicing systems using energy foundations. In Geo-Congress 2014: Geo-characterization and Modeling for Sustainability (pp. 2705-2714).

Chapman, W. P. (1952). Design of snow melting systems. Heating and Ventilating, 49(4), 96-102.

Chapman, W. P. (1957). Calculating the heat requirements of a snow melting system. Air Conditioning, Heating and Ventilating, 96.

Chiasson, A. D., Spitler, J. D., Rees, S. J., & Smith, M. D. (2000). A model for simulating the performance of a pavement heating system as a supplemental heat rejecter with closed-loop ground-source heat pump systems. Journal of Solar Energy Engineering-Transactions of The ASME, 122(4), 183-191.

Habibzadeh-Bigdarvish, O., Yu, X., Lei, G., Li, T., & Puppala, A. J. (2019). Life-Cycle cost-benefit analysis of Bridge deck de-icing using geothermal heat pump system: A case study of North Texas. Sustainable Cities and Society, 47, 101492.

Lucid Learning. (2017, Jan 24). Heat Diffusion Equation. Retrieved July 30, 2019, from https://medium.com/@lucidlearning314/general-heat-conduction-equation-cartesian-coordinates-9be71b546b76

Hurley, M. (2019). Performance Of Concrete Slabs With Embedded Hydronic Loops For Geothermally Based Bridge De-Icing Applications (Master's Thesis).

Kilkis, I.B., (1994a). Design of Embedded Snow Melting Systems: Part 1, Heat Requirements – An

Overall Assessment and Recommendations. ASHRAE Transaction, 100(1): 423-433.

Kilkis, I.B., (1994b). Design of Embedded Snow Melting Systems: Part 2, Heat Transfer in the Slab – A Simplified Model. ASHRAE Transactions, 100(1): 434-441.

Kosky, P., Balmer, R. T., Keat, W. D., & Wise, G. (2015). Exploring engineering: an introduction to engineering and design. Academic Press.

Leal, M. R. L. V., & Miller, P. L. (1972). Analysis of transient temperature distribution in pavement heating installations. In ASHRAE Journal-American Society Of Heating Refrigerating And Air-Conditioning Engineers (Vol. 14, No. 6, p. 35).

Lei, G., Kaneza, N., Yu, X., Li, T., & Habibzadeh-Bigdarvish, O. (2019). Development of a One-Dimensional Heating Soil Test Cell. Geo-Congress 2019: Geotechnical Materials, Modeling, and Testing, 682–690. American Society of Civil Engineers Reston, VA.

Li, T., Lei, G., Yu, X., Zhang, N., & Puppala, A. J. (2018). Numerical feasibility study of an externally heated geothermal bridge deck. In IFCEE 2018 (pp. 758-767).

Liu, X. (2005). Development and experimental validation of simulation of hydronic snow melting systems for bridges(Doctoral dissertation, Oklahoma State University).

Ramsey, J. W., Hewett, M. J., Kuehn, T. H., & Petersen, S. D. (1999). Updated design guidelines for snow melting systems. Ashrae Transactions, 105, 1055.

Rees, S. J., Spitler, J. D., & Xiao, X. (2002). Transient analysis of snow-melting system performance. ASHRAE Transactions, 108(2), 406-423.

Schnurr, N. M., & Rogers, D. B. (1970). Heat transfer design data for optimization of snow melting systems. In ASHRAE JOURNAL (Vol. 12, No. 6, p. 42).

Schnurr, N. M., & Falk, M. W. (1973). Transient analysis of snow melting systems. ASHRAE Transactions, 79(2), 159-166.

Spitler, J. D., Rees, S. J., & Liu, X., (2001). Quarterly Progress Report of the Oklahoma State University Smart Bridge Project. Oklahoma State University. Stillwater, OK.

Wikipedia contributors. (2019, May 18). Radiosity (radiometry). In Wikipedia, The Free Encyclopedia. Retrieved, July 10, 2019, from

https://en.wikipedia.org/w/index.php?title=Radiosity_(radiometry)&oldid=897691267

Williams, G.P., (1973). Heat Requirements of Snow Melting Systems in Canada. Proc., National Conference on Snow and Ice Control. Roads and Transportation Association of Canada, Ottawa, April 1973, P. 179-197.

Williams, G.P., (1976). Design heat requirements for embedded snow-melting systems in cold climates. Transportation Research Record, 576: 20-32.

Zhang, N., Yu, X., & Li, T. (2017). Numerical simulation of geothermal heated bridge deck. DEStech Transactions on Materials Science and Engineering, (ictim).

BIOGRAPHICAL INFORMATION

Mandakini completed her bachelor's in civil engineering from National Institute of Technology (NIT), Durgapur, India in May 2012. After her graduation, she joined Design Source Team, a structural consultant firm, as a structural engineer in Bangladesh, before joining The University of Texas at Arlington in Spring 2018 for her graduate studies. Her research interests include numerical modelling, structural design and behavior of soils and foundations.